ANO : FASTER IS BETTER IN NOISY LANDSCAPES

Adrien Kegreisz
Independent Researcher
Paris, France
adrien.kegreisz@gmail.com

ABSTRACT

Stochastic optimizers are central to deep learning, yet widely used methods such as Adam and Adan can degrade in non-stationary or noisy environments, partly due to their reliance on momentum-based magnitude estimates. We introduce Ano, a novel optimizer that decouples direction and magnitude: momentum is used for directional smoothing, while instantaneous gradient magnitudes determine step size. This design improves robustness to gradient noise while retaining the simplicity and efficiency of first-order methods. We further propose Anolog, which removes sensitivity to the momentum coefficient by expanding its window over time via a logarithmic schedule. We establish non-convex convergence guarantees with a convergence rate similar to other sign-based methods, and empirically show that Ano provides substantial gains in noisy and non-stationary regimes such as reinforcement learning, while remaining competitive on low-noise tasks such as standard computer vision benchmarks.

1 INTRODUCTION

Stochastic optimization is central to modern deep learning. Adaptive methods such as Adam (Kingma & Ba, 2015), and their variants (Reddi et al., 2018; Loshchilov & Hutter, 2019; Zaheer et al., 2018) are widely used because they automatically adjust step sizes and often accelerate early training. However, their behavior can degrade under noisy or non-stationary conditions: mini-batch stochasticity and data augmentation induce gradient noise (Mandt et al., 2017; Smith et al., 2018), labels may be ambiguous or noisy (Zhang et al., 2017; Song et al., 2022), and in reinforcement learning the training targets evolve over time (Henderson et al., 2019; Mnih et al., 2015). A common thread across these methods is their reliance on momentum estimates for both update direction and magnitude (Balles & Hennig, 2018). This entanglement makes them vulnerable: momentum magnitudes shrink in noisy regimes (Li et al., 2025), yielding overly conservative steps, or drift when noisy gradients accumulate (Bengio et al., 2021).

We propose **A New Optimizer**, abbreviated as **Ano**, which decouples direction and magnitude. Updates follow the sign of the momentum to benefit from its stability, while the step size is scaled by instantaneous gradient magnitudes, normalized by a variance term as in Adam. Intuitively, this design preserves the denoising benefits of momentum while enlarging the effective update to decorrelate the momentum.

We summarize our main contributions as follows:

- We propose a new gradient-scaling mechanism that removes the reliance on momentum-based magnitude estimates, leading to better adaptation in non-stationary and/or noisy optimization landscapes with the same memory cost as Adam.
- We provide a theoretical analysis of Ano in the non-convex setting, establishing a convergence rate of $\mathcal{O}\big(k^{-1/4}\big)$ under standard assumptions, matching existing results for sign-based optimizers.
- We evaluate Ano on supervised learning and deep reinforcement learning tasks, demonstrating substantial gains in noisy and non-stationary settings such as reinforcement learn-

ing, while remaining competitive in low-noise domains such as standard supervised benchmarks.

2 Related Work

Research on stochastic optimizers spans several directions. We briefly review the lines most relevant to Ano and situate our contribution.

Adaptive methods. AdaGrad (Duchi et al., 2011), AdaDelta (Zeiler, 2012) and RMSProp (Tieleman & Hinton, 2012) pioneered coordinate-wise adaptivity; Adam (Kingma & Ba, 2015) combined first- and second-moment estimates and became a default in deep learning. Yogi (Zaheer et al., 2018) stabilizes the second-moment accumulator for non-stationary regimes. More recently, Adan (Xie et al., 2024) couples adaptive moments with Nesterov-style lookahead and has emerged as a competitive baseline. Our optimizer Ano relates to this family through variance-aware step-size control, but differs in how direction and magnitude are constructed (see below).

Sign-based methods. SignSGD and Signum (Bernstein et al., 2018) reduce updates to element-wise signs, offering scale invariance and communication efficiency in distributed settings. Lion (Chen et al., 2023) revisits sign-based updates with a tailored momentum schedule, yielding strong empirical results. Ano keeps the robustness of sign-informed directions but reintroduces gradient magnitudes through an explicit decoupling, trading pure scale invariance for finer adaptivity.

Direction–magnitude decoupling. Recent works such as Grams (Cao et al., 2025) decouple the update by using gradient signs for direction and the momentum norm for scaling. Ano adopts a complementary design: momentum provides a stable directional signal, while the raw gradient norm sets the step size. This hybridization aims to combine the resilience of sign-based directions with the adaptivity of moment estimators.

Discussion. Overall, Ano bridges sign-based and adaptive-moment families through a novel direction–magnitude decoupling strategy, where momentum is used to denoise and stabilize directions while gradient magnitudes preserve sensitivity to local curvature. This positioning explains its empirical robustness on high-variance RL tasks while remaining competitive in more stable regimes.

3 Algorithm

Motivation and Intuition. In high-variance settings, optimizers like Adam rely on momentum to smooth updates through sharp minima and maxima. However, when gradient variance is high, the exponential moving average used for momentum can become dampened by noise, causing its magnitude to shrink and updates to become overly conservative. In addition, momentum may accumulate noisy, misaligned gradients, leading the update direction to drift away from the true descent path.

Momentum works best when it averages less correlated gradients that are at sufficiently different points in parameter space (Hermant et al., 2025). If updates are small, consecutive gradients are nearly identical and dominated by noise, making momentum unreliable. By using $|g_{k,i}|$ that tends to yield larger steps than $|m_{k,i}|$, we deliberately enlarge updates in noisy regions, while the normalization by $\sqrt{v_k}$ tempers outliers. This decorrelates successive gradients, enabling momentum to track the underlying descent direction more faithfully, while still permitting smooth progress in less noisy zones. Ano algorithm is presented below:

Algorithm 1: Ano Algorithm

Input: Initial parameters $x_1 \in \mathbb{R}^d$, learning rate η_k, decay rates $\beta_1, \beta_2 \in [0, 1)$, $\epsilon > 0$

Initialize $m_0 = 0$, $v_0 = 0$
for $k = 1$ **to** K **do**
  Compute gradient $g_k = \nabla \ell(x_k)$
  $m_k = \beta_1 m_{k-1} + (1 - \beta_1) g_k$
  $v_k = v_{k-1} - (1 - \beta_2) \cdot \text{sign}(v_{k-1} - g_k^2) \cdot g_k^2$
  $x_{k+1} = x_k - \frac{\eta_k}{\sqrt{v_k + \epsilon}} \cdot |g_k| \cdot \text{sign}(m_k) - \eta_k \lambda x_k$

Second-Moment Term. Throughout this work, we employ Yogi's additive update rule (Zaheer et al., 2018) to maintain the second-moment estimate:

$$v_k = v_{k-1} - (1 - \beta_2) \operatorname{sign}(v_{k-1} - g_k^2)\, g_k^2,$$

rather than Adam's exponential moving average. This adjustment prevents abrupt increases in effective learning rates when v_{t-1} significantly exceeds the current squared gradient, a known issue causing potential convergence instability. Empirically, this additive rule results in smoother loss curves, particularly in sparse-gradient scenarios, without additional memory or computational overhead. Thus, we adopt it as our default second-moment estimator.

Sign–Magnitude Decoupling. Inspired by recent optimizers like Lion (Chen et al., 2023) and Signum (Bernstein et al., 2018), we explicitly decouple the direction and magnitude signals of parameter updates.

Concretely, recall that Adam updates parameters via

$$x_{k+1} = x_k - \frac{\eta}{\sqrt{v_k} + \epsilon} \cdot m_k = x_k - \frac{\eta}{\sqrt{v_k} + \epsilon} \underbrace{|m_k|}_{\text{magnitude}} \cdot \underbrace{\text{sign}(m_k)}_{\text{direction}}.$$

Our optimiser **Ano** performs the same directional move but replaces the momentum magnitude with $|g_k|$:

$$x_{k+1} = x_k - \frac{\eta}{\sqrt{v_k} + \epsilon} \underbrace{|g_k|}_{\text{magnitude}} \cdot \underbrace{\text{sign}(m_k)}_{\text{direction}}.$$

Bias Correction and Weight Decay. Since Ano relies solely on the momentum direction for updates, bias correction of its magnitude is unnecessary and omitted for simplicity (same as Lion). For the second moment estimator, we follow Yogi algorithm so we don't use any bias correction. We therefore follow AdamW (Loshchilov & Hutter, 2019) and apply decoupled weight decay independently of gradient normalization.

Hyperparameters. Like AdamW, Ano maintains first and second moments estimators : m_k and v_k, each regulated by decay rates β_1 and β_2, with $\beta_i \in [0, 1)$. We set $\beta_1 = 0.92$ and $\beta_2 = 0.99$ for stable convergence. Additionally, a weight decay coefficient $\lambda \in [0, +\infty)$ is employed to mitigate overfitting.

4 EXTENSION

Inspired by our convergence analysis, we extend Ano to include a time-dependent momentum parameter β_1, resulting in a variant we denote **Anolog** (Ano with logarithmic scheduling). While Ano consistently yields the best raw performance, Anolog provides a practical advantage by removing the need to tune β_1. This reduction in hyperparameter sensitivity makes Anolog a competitive choice in scenarios with limited tuning budgets, despite its slightly lower peak performance.

We define $\beta_{1,k} = 1 - \frac{1}{\log(k+2)}$, following theoretical and experimental motivations that favor slow and progressive adjustments to optimization hyperparameters. A slowly increasing β_1 progressively enlarges the effective averaging window of the momentum, reducing the influence of stochastic

gradient noise as training progresses. In contrast, more aggressive schedules (e.g., square-root) can make the momentum insufficiently sensitive to recent gradient information, especially in the early iterations. We provide both empirical and ablation evidence in Section 7 to support the superiority of this scheduling choice against a square-root scheduling ($\beta_{1,k} = 1 - \frac{1}{\sqrt{k}}$) or a harmonic scheduling ($\beta_{1,k} = 1 - \frac{1}{k}$).

Full Anolog pseudo code can be found in Appendix A.

5 Analysis

5.1 Theoretical Analysis

We provide non-asymptotic convergence guarantees for **Ano** under standard assumptions commonly used in adaptive stochastic optimisation (Kingma & Ba, 2015; Reddi et al., 2018). Consider the stochastic optimisation problem: $\min_{x\in\mathbb{R}^d} f(x)$, where f is differentiable, L-smooth, and bounded below. Let $g_{k,i}$ denote the i-th coordinate of the stochastic gradient at iteration k and $\mathcal{F}_{k-1}$ the filtration k-1. We assume that the gradient is bounded, $\|\nabla f(x)\| \leq G, \forall x \in \mathbb{R}^d$, the stochastic gradient is unbiased ($\mathbb{E}[g_{k,i} \mid \mathcal{F}_{k-1}] = \nabla_i f(x_k)$), and the variance is bounded ($\mathbb{E}[(g_{k,i} - \nabla_i f(x_k))^2 \mid \mathcal{F}_{k-1}] \leq \sigma^2$).

Main result. Following recent convergence analyses of sign-based optimizers, especially Lion (Dong et al., 2024), we assume a learning-rate schedule $\eta_k = \eta/k^{3/4}$ and $\beta_{1,k} = 1 - 1/\sqrt{k}$, the iterates generated by **Ano** satisfy:

$$\min_{0\leq k<K} \mathbb{E}[\|\nabla f(x_k)\|^2] \;=\; \mathcal{O}(K^{-1/4}\log K) \;=\; \tilde{\mathcal{O}}(K^{-1/4}),$$

up to logarithmic factors, in the general non-convex stochastic setting.

Proof sketch. Using a sign-mismatch lemma (Lemma 1, Appendix C), we show that the probability of momentum–gradient disagreement decays as $\mathcal{O}(1/\sqrt{k})$. Then, using L-smoothness and the previous lemma, we establish the inequality:

$$\mathbb{E}[f(x_{k+1})] \;\leq\; \mathbb{E}[f(x_k)] \;-\; \frac{\eta_k}{\sqrt{2}G+\varepsilon}\,\mathbb{E}[\|\nabla f(x_k)\|^2] \;+\mathcal{O}\Big(\frac{\eta_k}{k^{1/4}}\Big) \;+\mathcal{O}(\eta_k^2),$$

where the last two terms represent, respectively, stochastic noise and the adaptivity of the step size.

Discussion. Our bound matches those recently established for sign-based optimizers such as *Lion*(Dong et al., 2024) and *Signum*(Bernstein et al., 2018), while relying on less restrictive assumptions (e.g., no requirement for growing batch sizes).Compared to adaptive schemes (SGD, Adam, Yogi) achieving $\mathcal{O}(K^{-1/2})$, our $\tilde{\mathcal{O}}(K^{-1/4})$ rate reflects a robustness–efficiency trade-off: Ano prioritizes stable sign-based updates, enforced by decaying schedules $\eta_k = \mathcal{O}(k^{-3/4})$ and $\beta_{1,k} = 1 - 1/\sqrt{k}$. Full proofs are in Appendix C.

5.2 Noise Robustness Analysis

We assess noise robustness by training a CIFAR-10 CNN adding Gaussian noise $g_k \leftarrow g_k + \mathcal{N}(0, \sigma^2)$ into every mini-batch gradient before the optimizer update. We vary only the noise level σ over five values, keep each optimizer's default β and recommended learning rate (Full hyperparameters tabs can be found in Appendix B) for a computer vision task and report mean test accuracy over 5 seeds.[1]

The performance gap between Ano/Adam and Ano/Lion widens with noise magnitude, reaching a -6.8-point advantage at $\sigma = 0.20$ for Adam and a -2.7-point advantage for Lion(Table 1). Another noteworthy observation is that Grams improves with a small injected noise ($\sigma = 0.01$). We hypothesize that this injected perturbation amplifies short-term oscillations, enlarging its second-moment (variance) estimate and thereby shrinking the step size, allowing Grams to refine its iterates more

[1]Standard deviations omitted here for readability. The full table with standard deviation is available in Appendix D - tab 7

Optimizer	$\sigma = 0$	0.01	0.05	0.10	0.20
Ano	82.25	78.78	71.03	65.96	59.81
Adam	80.89(**-1.36**)	76.08(**-2.7**)	66.43(**-4.6**)	60.56 (**-5.4**)	53.01(**-6.8**)
Lion	81.23(**-1.02**)	77.69(**-1.09**)	69.40(**-1.63**)	64.03(**-1.93**)	57.07(**-2.74**)
Grams	71.37(**-10.88**)	77.91(**-0.87**)	70.56(**-0.47**)	65.47(**-0.49**)	58.8(**-1.01**)

Table 1: CIFAR-10 test accuracy (%). Numbers in parentheses indicate the gap (percentage points) relative to *Ano*.

cautiously in a noisy landscape. Overall, these results support our central claim that decoupling update direction from magnitude stabilizes learning under high variance, avoiding the over-smoothing of momentum-coupled schemes.

6 Experiments

We benchmark **Ano** and its extension **Anolog** against established optimizers and similar optimizers across computer vision, natural language processing, and deep reinforcement learning. Hyperparameters for all methods are selected via per-domain (DRL, CV, NLP) proxy grid searches: each optimizer receives a fixed 40 GPU-hour budget centered on litterature defaults(cf Appendix B). Final results are averaged over 5 seeds for CV/NLP and 10 for DRL. Full search spaces, selected configurations, logs and codes are released (Appendices B-E.1).

6.1 Computer Vision

Computer vision is a historically important domain for benchmarking optimization algorithms. In this section, we evaluate Ano on CIFAR-100 (Krizhevsky, 2009) using ResNet-34 (He et al., 2015).

CIFAR-100. We use the standard CIFAR augmentation (random crop with 4-pixel padding + horizontal flip), following Zagoruyko & Komodakis (2017).

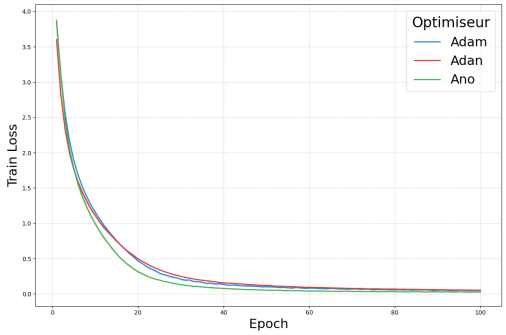

Figure 1: Training loss on CIFAR-100. Ano reduces loss faster and more stably than Adam.

Optimizers	Test Accuracy	Training Loss
Baseline		
Adam	69.92 ± 0.18	0.042
Adan	69.87 ± 0.09	0.052
Lion	64.99 ± 2.22	0.100
Grams	69.80 ± 0.10	0.047
Ano	$\mathbf{70.16 \pm 0.047}$	**0.024**
Tuned		
Adam	69.85 ± 0.10	0.045
Adan	70.53 ± 0.20	0.050
Lion	69.61 ± 0.13	0.051
Grams	69.82 ± 0.10	0.053
Ano	$\mathbf{71.15 \pm 0.31}$	**0.021**

Table 2: Test accuracy and training loss on CIFAR-100.

As shown in Table 2, **Ano** outperforms Adam and Adan in both default and tuned settings. Figure 1 further illustrates that Ano achieves faster convergence and lower training loss throughout training.

6.2 Transformers

As a cornerstone of modern artificial intelligence, natural language processing (NLP) warrants careful evaluation of optimization algorithms. The unique challenges of NLP, such as large parameter spaces, sparse gradients, and label noise, can affect optimizer performance (Mosbach et al., 2021). We assess the effectiveness of **Ano** by comparing it to standard baselines on the GLUE benchmark (Wang et al., 2019), covering eight sentence- and sentence-pair classification tasks (excluding WNLI, following standard practice due to its unreliable performance).

GLUE All runs finetune the public `bert-base-uncased` checkpoint (Devlin et al., 2019) with max sequence length 128, batch size 32, weight decay 0.01, linear schedule with 10% warmup, mixed precision, and 3 epochs (5 for small datasets: CoLA, MRPC, RTE, STS-B). Each configuration is repeated over 5 seeds.

Optimizer	CoLA	MNLI	MRPC	QNLI	QQP	RTE	SST-2	STS-B	Average
Baseline									
AdamW	$\mathbf{59.40 \pm 1.67}$	$\mathbf{84.62 \pm 0.10}$	88.06 ± 0.82	$\mathbf{91.60 \pm 0.15}$	89.64 ± 0.10	66.67 ± 1.59	92.73 ± 0.46	88.44 ± 0.27	82.64
Adan	55.65 ± 0.53	84.17 ± 0.07	84.40 ± 0.83	91.10 ± 0.14	88.85 ± 0.04	61.49 ± 1.30	92.02 ± 0.20	87.26 ± 0.63	80.62
Lion	57.76 ± 1.76	83.76 ± 0.23	87.13 ± 0.81	90.63 ± 0.68	89.46 ± 0.05	62.89 ± 1.17	91.67 ± 0.52	88.00 ± 0.25	81.41
Grams	56.15 ± 0.92	83.89 ± 0.11	84.92 ± 0.60	91.10 ± 0.04	88.48 ± 0.08	63.36 ± 1.60	92.34 ± 0.19	87.57 ± 0.32	80.98
Ano (Ours)	58.36 ± 1.15	84.33 ± 0.17	$\mathbf{88.96 \pm 0.50}$	91.25 ± 0.46	$\mathbf{89.71 \pm 0.11}$	$\mathbf{69.25 \pm 2.94}$	$\mathbf{92.80 \pm 0.41}$	88.70 ± 0.12	**82.92**
Anolog (Ours)	57.07 ± 2.41	84.55 ± 0.09	88.26 ± 0.76	91.51 ± 0.10	$\mathbf{89.71 \pm 0.12}$	67.87 ± 1.94	92.75 ± 0.15	$\mathbf{88.95 \pm 0.32}$	82.58
Tuned									
AdamW	57.66 ± 2.39	84.18 ± 0.16	88.09 ± 0.79	91.12 ± 0.17	89.55 ± 0.08	68.47 ± 2.91	92.18 ± 0.08	88.76 ± 0.36	82.50
Adan	57.71 ± 0.92	$\mathbf{84.84 \pm 0.10}$	88.14 ± 0.40	91.71 ± 0.21	$\mathbf{89.78 \pm 0.07}$	65.40 ± 1.66	92.68 ± 0.26	88.57 ± 0.44	82.35
Lion	56.30 ± 0.55	82.38 ± 0.06	86.83 ± 2.91	90.36 ± 0.42	88.60 ± 0.13	63.75 ± 5.50	91.47 ± 0.24	88.58 ± 0.40	81.03
Grams	58.18 ± 1.12	84.64 ± 0.11	$\mathbf{89.05 \pm 0.36}$	$\mathbf{91.79 \pm 0.17}$	89.66 ± 0.06	67.22 ± 2.55	$\mathbf{92.98 \pm 0.31}$	88.53 ± 0.26	82.76
Ano (Ours)	$\mathbf{58.51 \pm 0.75}$	84.39 ± 0.12	88.53 ± 1.14	91.30 ± 0.48	89.73 ± 0.07	$\mathbf{69.25 \pm 3.01}$	92.66 ± 0.14	88.74 ± 0.11	**82.89**
Anolog (Ours)	57.07 ± 2.41	84.55 ± 0.09	88.26 ± 0.76	91.51 ± 0.10	89.71 ± 0.12	67.87 ± 1.94	92.75 ± 0.15	$\mathbf{88.95 \pm 0.32}$	82.58

Table 3: Average performance (mean $\pm$ 95% CI) of different optimizers on GLUE benchmark tasks (best per column in bold).

As shown in Table 3, **Ano** and its logarithmic version (**Anolog**) achieve the highest average score across GLUE. This improvement is mainly driven by its performance on small-scale and inherently noisy tasks such as MRPC, CoLA and RTE, which are known to exhibit high gradient variance. These results suggest that Ano's advantages are most pronounced on noisy, low-resource tasks as we can expect.

6.3 Deep Reinforcement learning

Reinforcement learning (RL) poses unique challenges, including high gradient variance and the non-stationarity of the environment, both of which can impact the performance of optimization algorithms. Consequently, optimizers that demonstrate strong performance in domains such as natural language processing may behave quite differently in RL settings (Henderson et al., 2019; François-Lavet et al., 2018). This is precisely the domain where Ano is designed to achieve its most significant gains. To evaluate our algorithms, we adopt the MuJoCo suite from the Gymnasium framework developed by the Farama Foundation (Todorov et al., 2012; Towers et al., 2024).

Soft-Actor Critic. In this section, we employ the Soft Actor-Critic (SAC) algorithm (Haarnoja et al., 2018). We reuse the standard SAC hyperparameter (full list in Appendix E.1 - Tab 11), as reported in the original work and subsequent studies and only vary the optimizer for actor, critics, and temperature. For each optimizer, we run 10 seeds, with 1M steps. We report below the average mean score over the 20 final runs at the end of the training.

Optimizers	HalfCheetah	Ant	Humanoid	Walker2d	Hopper	Mean Rank	Norm. Avg
Baseline							
Adam	9477.97 ± 1003.20	4161.08 ± 515.06	$\mathbf{5247.63 \pm 105.87}$	4276.75 ± 238.68	2922.12 ± 284.42	2.6	90.01
Adan	8796.97 ± 955.18	3294.58 ± 433.50	5116.14 ± 125.19	3698.10 ± 572.68	2509.11 ± 324.34	4.8	79.87
Lion	7406.13 ± 2772.84	3491.82 ± 579.52	85.58 ± 28.33	4768.21 ± 201.84	703.34 ± 657.37	4.6	50.72
Grams	6457.31 ± 879.37	3031.85 ± 478.99	5181.55 ± 105.09	3386.75 ± 896.29	2606.07 ± 579.75	4.8	74.25
Ano (Ours)	$\mathbf{10851.8 \pm 518.67}$	$\mathbf{5247.02 \pm 653.98}$	5190.86 ± 136.30	$\mathbf{5119.08 \pm 420.88}$	$\mathbf{2926.39 \pm 308.72}$	**1.2**	**99.78**
Anolog (Ours)	10389.5 ± 1041.29	4598.67 ± 727.16	5161.95 ± 268.91	4748.18 ± 593.57	2585.67 ± 238.48	3.0	92.57
Tuned							
Adam	9874.24 ± 735.62	4110.11 ± 692.96	$\mathbf{5308.70 \pm 195.70}$	4369.92 ± 326.27	$\mathbf{3143.48 \pm 233.52}$	2.6	90.43
Adan	10133.64 ± 849.35	5222.12 ± 218.59	5034.40 ± 95.83	$\mathbf{4981.25 \pm 184.94}$	2971.66 ± 367.72	2.4	95.35
Lion	7351.97 ± 3058.09	2826.41 ± 1698.65	86.81 ± 24.43	4496.17 ± 519.54	430.78 ± 260.73	4.6	44.74
Grams	8522.14 ± 1648.23	4187.69 ± 707.71	5116.82 ± 135.39	4204.40 ± 836.06	2870.06 ± 740.79	3.6	85.18
Ano (Ours)	$\mathbf{11197.73 \pm 278.11}$	$\mathbf{5389.34 \pm 353.92}$	5071.59 ± 138.17	4810.42 ± 356.80	2972.84 ± 418.39	**1.8**	**97.34**

Table 4: Comparison of the average performance (± 95% CI) of different optimizers across environments.

As summarized in Table 4, Ano performs favorably compared to Adam and other baselines across the MuJoCo tasks. On average, it achieves a **+10%** improvement in normalized score[2], both under

[2]The normalized average is obtained by linearly rescaling each score between the minimum and maximum values observed across optimizers, followed by averaging. Complete normalized results are reported in Table 8.

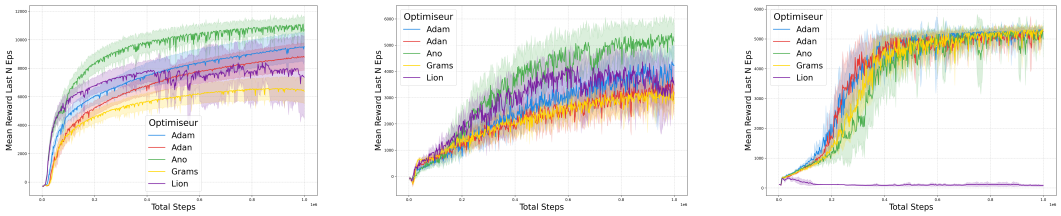

(a) Halfcheetah-v5 (b) Ant-v5 (c) Humanoid-v5

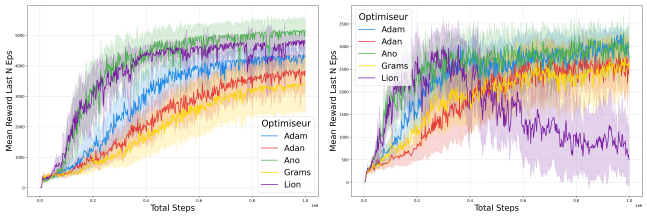

(d) Walker2d-v5 (e) Hopper-v5

Figure 2: Rewards over time for several MuJoCo environments, with baselines and 95% confidence intervals. The green curve corresponds to **Ano (ours)**.

default and tuned hyperparameters. Without tuning, Ano ranks first in 4 out of 5 tasks; with tuning, it remains the top optimizer in 2 out of 5 tasks. Although not always the best performer, Ano consistently ranks among the strongest optimizers, with its scores typically within or close to the 95% confidence intervals of the best baselines. Figure 2 shows that Ano converges faster, reaching Adam's final performance in roughly 70% of the training steps. In contrast, Lion and Grams exhibit pronounced instability on high-variance tasks such as Humanoid, while Anolog, our ablated variant—remains competitive but consistently lags behind Ano. To further address potential concerns about hyperparameter tuning, we evaluated sensitivity to the learning rate and momentum coefficients on HalfCheetah (Figure 3) on a 100k steps HalfCheetah proxy. Ano exhibits markedly lower sensitivity than Adam on learning rate and betas, suggesting that its advantage is not merely due to more favorable hyperparameters.

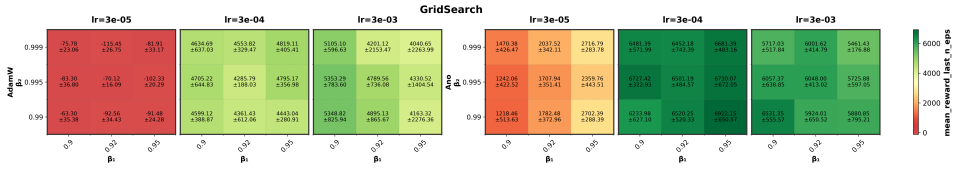

Figure 3: Hyperparameter robustness on a MuJoCo proxy (HalfCheetah with SAC). **Adam** on the left, **Ano(ours)** on the right.

Proximal Policy Optimization. To assess the generality of our findings, we additionally evaluate a discrete-action variant of Proximal Policy Optimization (PPO) (Schulman et al., 2017) on the Atari Learning Environment (ALE) (Bellemare et al., 2013). For compute efficiency, we report results on the *Atari-5* subset proposed by Aitchison et al. (Aitchison et al., 2022), which explains 98.4% of the variance in full-suite performance (R^2=0.984). We use the reference PPO implementation from CleanRL (Huang et al., 2022) and keep its default network and optimization hyperparameters (full list in Appendix E.1 - tab 12). Environments are instantiated via EnvPool (Weng et al., 2022) for fast batched simulation. Observations are resized to 84×84, converted to grayscale, and stacks of 4 consecutive frames are fed to the agent. We apply action repeat of 4, up to 30 no-op actions at reset, the ALE sticky-action protocol with repeat probability 0.25 (Machado et al., 2017), and FireReset where required. We used the full action set. During training, rewards are clipped to $[-1, 1]$; evaluation uses unclipped rewards. We train for 10M agent steps (with action repeat 4, i.e., $\approx$ 40M ALE frames), evaluating every 200k steps on 50 runs. Each checkpoint is evaluated with

the same wrappers as training (except reward clipping). We report the average final score on the last evaluation. The normalization average is computed in the same ways that previous part[3].

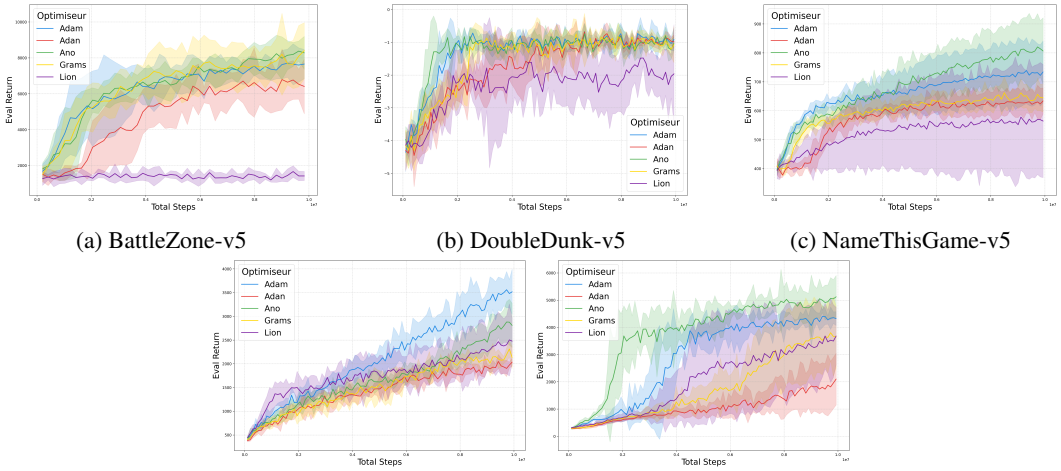

(a) BattleZone-v5 (b) DoubleDunk-v5 (c) NameThisGame-v5

(d) Phoenix-v5 (e) Qbert-v5

Figure 4: Rewards over time for Atari5 Benchmark, with baselines and 95% confidence intervals. The green curve corresponds to **Ano (ours)**.

Optimizers	BattleZone-v5	DoubleDunk-v5	NameThisGame-v5	Phoenix-v5	Qbert-v5	Mean Rank	Norm. Avg
Baseline							
Adam	7656.00 ± 812.20	$\mathbf{-0.91} \pm 0.34$	733.92 ± 107.34	$\mathbf{3516.64} \pm 475.14$	4322.00 ± 254.93	2.2	92.40
Adan	6408.00 ± 1525.14	-0.98 ± 0.21	633.80 ± 44.93	2033.76 ± 85.42	2100.60 ± 951.20	4.8	70.22
Lion	1420.00 ± 256.88	-1.96 ± 1.50	564.44 ± 195.39	2477.12 ± 490.65	3680.80 ± 1057.34	5.2	63.83
Grams	$\mathbf{8396.00 \pm 1565.13}$	-1.07 ± 0.55	644.64 ± 48.73	2133.76 ± 234.64	3646.70 ± 1139.41	3.8	81.41
Ano (Ours)	8280.00 ± 916.31	-1.03 ± 0.21	$\mathbf{806.56 \pm 114.49}$	2808.68 ± 465.32	5122.12 ± 783.72	**2.2**	**94.48**
Anolog (Ours)	7620.00 ± 1225.14	-1.07 ± 0.26	743.00 ± 191.30	2815.50 ± 430.55	$\mathbf{5413.75 \pm 1873.65}$	2.8	92.40
Tuned							
Adam	7880.00 ± 1218.48	$\mathbf{-0.93 \pm 0.15}$	663.87 ± 178.56	2964.16 ± 601.40	4222.90 ± 256.83	2.6	90.51
Adan	4672.00 ± 2542.63	-1.08 ± 0.27	693.96 ± 87.13	$\mathbf{3020.48 \pm 419.22}$	4540.20 ± 996.34	2.6	86.03
Lion	1296.00 ± 164.16	-2.73 ± 1.92	550.96 ± 134.29	2554.80 ± 546.74	3267.00 ± 915.37	4.8	65.14
Grams	7536.00 ± 240.38	-1.41 ± 0.46	704.68 ± 123.61	1864.92 ± 204.72	4962.38 ± 1373.46	3.2	85.91
Ano (Ours)	$\mathbf{9556.00 \pm 2370.99}$	-1.13 ± 0.43	$\mathbf{733.95 \pm 235.51}$	2862.24 ± 365.46	$\mathbf{5181.70 \pm 1210.60}$	**1.8**	**98.72**

Table 5: Comparison of the average performance (± IC95%) of different optimizers across Atari environments.

As shown in Table 5, Ano and Adam are the strongest overall baselines. In the untuned setting, their mean ranks are 2.2 and 2.4; with tuning, 1.8 and 2.8, respectively. Ano attains the best average normalized score and the best mean rank in both regimes. A per-game breakdown indicates that Ano outperforms Adam on *BattleZone*, *Name This Game*, and *Q*bert*, whereas Adam clearly leads on *Phoenix*. For *DoubleDunk*, all optimizers (except Lion) saturate in the same plateau region (Fig. 4b), so no clear winner emerges. Interestingly, Adam performs slightly worse under our tuned configuration than under its default hyperparameters (β_1=0.9, β_2=0.999). Our tuned settings were obtained via a grid search on MuJoCo with SAC and then transferred to Atari PPO (Appendix B), following the common practice that PPO and SAC often share learning-rate and momentum parameters. This transfer appears more benign for Ano benefiting from $\beta_1 = 0.95$, than for Adam, suggesting greater hyperparameter sensitivity of the latter.

7 Ablation Study

We conduct ablation studies on Ano and on its variant Anolog to quantify the contribution of each design component and, in particular, to justify adopting a logarithmic momentum schedule instead of a theoretically motivated square-root schedule.

[3]We normalized each score by environment by the theoretically minimum (-18 for DoubleDunk, 0 for the others) and the maximum score obtained by the baselines, we then compute the mean average normalized score.

Table 6 lists all ablated variants. We compared the performance across four benchmarks: deep reinforcement learning (HalfCheetah-v5), computer vision, and two NLP classification tasks—MRPC (relatively noisy) and SST-2 (more stable).

Optimizer	Base LR	Adam Adapt.	Yogi Adapt.	Grad. Norm	Mom. Norm	Mom. Dir.	Decoup. WD	$\beta_{1,k}$	Score DRL	Acc. (%) CIFAR-100	Acc. (%) MRPC	Acc. (%) SST-2
Ano ablation												
Adam	✗	✓	✗	✗	✓	✓	✓	β_1	8048.02 ± 1323.36	69.73 ± 0.30	86.03 ± 1.66	93.08 ± 0.54
Yogi	✗	✗	✓	✗	✓	✓	✓	β_1	8871.78 ± 671.222	70.57 ± 0.07	85.05 ± 2.17	92.81 ± 0.42
Grams	✗	✓	✗	✗	✓	✗	✓	β_1	5493.76 ± 782.37	70.20 ± 0.17	81.94 ± 1.16	92.28 ± 0.40
Yogi+Signum	✗	✗	✓	✗	✗	✓	✓	β_1	-260.91 ± 41.114	3.99 ± 2.01	68.38 ± 0.00	50.92 ± 0.00
Signum+WeightDecay	✓	✗	✗	✗	✗	✓	✓	β_1	8987.63 ± 1399.78	64.983 ± 1.59	86.03 ± 0.56	90.29 ± 0.27
Signum+WeightDecay+GradNorm	✓	✗	✗	✓	✗	✓	✓	β_1	–	53.63 ± 0.30	68.38 ± 0.00	53.33 ± 2.62
Adam+GradNorm	✗	✓	✗	✓	✗	✓	✓	β_1	9917.19 ± 1192.77	70.32 ± 0.64	86.52 ± 0.73	92.60 ± 1.01
Ours (Ano)	✗	✗	✓	✓	✗	✓	✓	β_1	$\mathbf{10823.5 \pm 416.07}$	69.64 ± 0.79	86.44 ± 0.85	92.66 ± 0.45
Anolog ablation												
Anoall	✗	✓	✗	✓	✗	✓	✓	$1 - 1/k$	-212.18 ± 22.25	29.48 ± 2.4	76.42 ± 3.38	74.00 ± 11.97
Anosqrt	✗	✓	✗	✓	✗	✓	✓	$1 - 1/\sqrt{k}$	8674.09 ± 1390.00	67.26 ± 0.41	85.78 ± 0.96	91.44 ± 0.50
Ours (Anolog)	✗	✗	✓	✓	✗	✓	✓	$1 - 1/\log k$	$\mathbf{9342.92 \pm 1652.96}$	67.00 ± 0.80	$\mathbf{86.961 \pm 1.181}$	92.93 ± 0.15

Table 6: Ablation of our proposed optimizer(**Ano**) and its extension (**Anolog**). Columns on the left indicate which components are active; columns on the right report mean performance $\pm$ 95% CI

As shown in Table 6, **Ano** achieves the highest mean return in deep reinforcement learning (10365.5 ± 513.5), representing an improvement of approximately 7% over the same algorithm using Adam-style second moments, and around 20% over **Yogi** and **Signum**, the strongest baselines. At the same time, Ano remains within 1% of the top accuracy on each supervised learning task. Performance degrades when either adaptive second-moment estimation or gradient normalization is removed, highlighting their complementary roles. Yogi-style second-moment updates outperform Adam-style ones in DRL and are therefore adopted. Regarding momentum schedules, the logarithmic schedule yields a 12% improvement in DRL return compared to the $\sqrt{k}$ schedule, without compromising classification accuracy, thus motivating its inclusion in the final design.

8 Limitations and Discussion

Through the design and empirical analysis of Ano, we identified two main limitations. First, explicitly scaling updates with the instantaneous gradient norm improves robustness under noise but can also cause overshooting when transient variance spikes inflate the step size before curvature feedback stabilizes the update. We tested simple magnitude clipping, but it did not provide consistent gains. Second, learning-rate heuristics inherited from Adam do not transfer directly: because Adam's momentum norm is typically smaller than the raw magnitude term used in Ano, the same nominal rate produces a larger effective step. In supervised vision tasks, we therefore recommend a smaller default (10^-4) instead of 10^-3, which yielded more stable convergence (see Appendix B). We also explored Nesterov-style acceleration in the spirit of Adan, but initial trials suggested that combining acceleration with magnitude-aware updates increased instability rather than mitigating it. Together, these limitations highlight the need for more stable handling of the magnitude component, for example through robust norm estimation or adaptive damping, so as to prevent overshooting while retaining Ano's resilience to noisy gradients.

9 Conclusion

We introduced **Ano**, an alternative to momentum-based adaptive optimizers that decouples direction and magnitude, improving robustness in noisy and non-stationary settings. Under standard smoothness and bounded-noise assumptions, we provide non-asymptotic guarantees comparable to prior analyses of sign-based methods (e.g., Signum, Lion) under similar decay schedules. Empirically, Ano delivers substantial gains in reinforcement learning and low-resource NLP tasks, while remaining competitive on low-noise tasks.

Despite these strengths, Ano can more easily overshoots due to its reliance on instantaneous magnitudes; in supervised settings we therefore recommend smaller learning rates (e.g., 10^{-4} rather than 10^{-3}), as discussed in Section 8. Future work will explore adaptive damping of the magnitude term, integration with Nesterov-style look-ahead, and extensions to large-scale foundation-model pre-training, with an eye toward dynamic hyperparameter adaptation.

10 REPRODUCIBILITY STATEMENT

The full source code (training, preprocessing, and result visualization), along with all the logs from our experiments, is available on the Github Repository [4]. The optimizer can also be imported by installing the library (PIP INSTALL ANO-OPTIMIZER) to facilitate the implementation. Data preprocessing methods are described in the relevant sections of the Experiments part (see Section 6) and are also in our source code. MuJoCo experiments were conducted on a MacBook Pro with an Apple M4 Pro chip (16-core GPU, 12-core CPU), while other experiments were run on a workstation equipped with an RTX 5090 GPU and an Intel Core Ultra 9 processor, using CUDA 12.9 and PyTorch 2.9.0. All software dependencies are specified in the requirements.txt included in the repository, ensuring exact reproducibility.

The total compute time for all experiments was approximately 2000 hours: about 125 hours for the ablation study7, 215 hours for hyperparameter tuningB, and 1700 hours for the main experiments reported in Section 6.

REFERENCES

Matthew Aitchison, Penny Sweetser, and Marcus Hutter. Atari-5: Distilling the arcade learning environment down to five games, 2022. URL https://arxiv.org/abs/2210.02019.

Lukas Balles and Philipp Hennig. Dissecting adam: The sign, magnitude and variance of stochastic gradients. In *Proceedings of the 35th International Conference on Machine Learning (ICML)*, volume 80 of *Proceedings of Machine Learning Research*, pp. 404–413, 2018. URL http://proceedings.mlr.press/v80/balles18a.html.

M. G. Bellemare, Y. Naddaf, J. Veness, and M. Bowling. The arcade learning environment: An evaluation platform for general agents. *Journal of Artificial Intelligence Research*, 47:253–279, June 2013. ISSN 1076-9757. doi: 10.1613/jair.3912. URL http://dx.doi.org/10.1613/jair.3912.

Emmanuel Bengio, Joelle Pineau, and Doina Precup. Correcting momentum in temporal difference learning, 2021. URL https://arxiv.org/abs/2106.03955.

Jeremy Bernstein, Yu-Xiang Wang, Kamyar Azizzadenesheli, and Anima Anandkumar. signsgd: Compressed optimisation for non-convex problems. In *Proceedings of the 35th International Conference on Machine Learning (ICML)*, volume 80 of *Proceedings of Machine Learning Research*, pp. 559–568, 2018. URL http://proceedings.mlr.press/v80/bernstein18a.html.

Yang Cao, Xiaoyu Li, and Zhao Song. Grams: Gradient descent with adaptive momentum scaling, 2025. URL https://arxiv.org/abs/2412.17107.

Xiangning Chen, Chen Liang, Da Huang, Esteban Real, Kaiyuan Wang, Yao Liu, Hieu Pham, Xuanyi Dong, Thang Luong, Cho-Jui Hsieh, Yifeng Lu, and Quoc V. Le. Symbolic discovery of optimization algorithms. In *Advances in Neural Information Processing Systems (NeurIPS)*, 2023. URL https://arxiv.org/abs/2302.06675.

Jacob Devlin, Ming-Wei Chang, Kenton Lee, and Kristina Toutanova. Bert: Pre-training of deep bidirectional transformers for language understanding, 2019. URL https://arxiv.org/abs/1810.04805.

Yiming Dong, Huan Li, and Zhouchen Lin. Convergence rate analysis of lion, 2024. URL https://arxiv.org/abs/2411.07724.

John Duchi, Elad Hazan, and Yoram Singer. Adaptive subgradient methods for online learning and stochastic optimization. *Journal of Machine Learning Research*, 12(61):2121–2159, 2011. URL http://jmlr.org/papers/v12/duchi11a.html.

[4] https://github.com/Adrienkgz/ano-experiments

Vincent François-Lavet, Peter Henderson, Riashat Islam, Marc G. Bellemare, and Joelle Pineau. An introduction to deep reinforcement learning. *Foundations and Trends® in Machine Learning*, 11 (3–4):219–354, 2018. ISSN 1935-8245. doi: 10.1561/2200000071. URL http://dx.doi.org/10.1561/2200000071.

Tuomas Haarnoja, Aurick Zhou, Pieter Abbeel, and Sergey Levine. Soft actor-critic: Off-policy maximum entropy deep reinforcement learning with a stochastic actor. In *Proceedings of the 35th International Conference on Machine Learning (ICML)*, pp. 1861–1870, 2018.

Kaiming He, Xiangyu Zhang, Shaoqing Ren, and Jian Sun. Deep residual learning for image recognition, 2015. URL https://arxiv.org/abs/1512.03385.

Peter Henderson, Riashat Islam, Philip Bachman, Joelle Pineau, Doina Precup, and David Meger. Deep reinforcement learning that matters, 2019. URL https://arxiv.org/abs/1709.06560.

Julien Hermant, Marien Renaud, Jean-François Aujol, Charles Dossal, and Aude Rondepierre. Gradient correlation is a key ingredient to accelerate sgd with momentum, 2025. URL https://arxiv.org/abs/2410.07870.

Shangmin Huang, Yash Chandak, Quan Vuong, Mengdi Fang, Stephen Scott, Carl Allen, Joshua Romoff, Tom Zahavy, Meng Sun, Arthur Guez, et al. Cleanrl: High-quality single-file implementations of deep reinforcement learning algorithms. *Journal of Machine Learning Research*, 23 (274):1–18, 2022.

Diederik P. Kingma and Jimmy Ba. Adam: A method for stochastic optimization. In *International Conference on Learning Representations (ICLR)*, 2015. URL https://arxiv.org/abs/1412.6980.

Alex Krizhevsky. Learning multiple layers of features from tiny images. Technical report, University of Toronto, 2009. URL https://www.cs.toronto.edu/~kriz/learning-features-2009-TR.pdf.

Xianliang Li, Jun Luo, Zhiwei Zheng, Hanxiao Wang, Li Luo, Lingkun Wen, Linlong Wu, and Sheng Xu. On the performance analysis of momentum method: A frequency domain perspective. In *International Conference on Learning Representations (ICLR)*, 2025. URL https://arxiv.org/abs/2411.19671. Sec. 3; shows attenuation of high-frequency components and smaller momentum norms.

Ilya Loshchilov and Frank Hutter. Decoupled weight decay regularization. In *International Conference on Learning Representations (ICLR)*, 2019. URL https://openreview.net/forum?id=Bkg6RiCqY7.

Marlos C. Machado, Marc G. Bellemare, Erik Talvitie, Joel Veness, Matthew Hausknecht, and Michael Bowling. Revisiting the arcade learning environment: Evaluation protocols and open problems for general agents, 2017. URL https://arxiv.org/abs/1709.06009.

Stephan Mandt, Matthew D. Hoffman, and David M. Blei. Stochastic gradient descent as approximate bayesian inference. *Journal of Machine Learning Research*, 18(134):1–35, 2017. URL http://www.jmlr.org/papers/v18/17-214.html.

Volodymyr Mnih, Koray Kavukcuoglu, David Silver, Andrei A. Rusu, Joel Veness, Marc G. Bellemare, Alex Graves, Martin Riedmiller, Andreas K. Fidjeland, Georg Ostrovski, Stig Petersen, Charles Beattie, Amir Sadik, Ioannis Antonoglou, Helen King, Dharshan Kumaran, Daan Wierstra, Shane Legg, and Demis Hassabis. Human-level control through deep reinforcement learning. *Nature*, 518(7540):529–533, February 2015. ISSN 1476-4687. doi: 10.1038/nature14236.

Marius Mosbach, Maksym Andriushchenko, and Dietrich Klakow. On the stability of fine-tuning bert: Misconceptions, explanations, and strong baselines, 2021. URL https://arxiv.org/abs/2006.04884.

Sashank J. Reddi, Satyen Kale, and Sanjiv Kumar. On the convergence of adam and beyond. In *International Conference on Learning Representations (ICLR)*, 2018. URL https://openreview.net/forum?id=ryQu7f-RZ.

John Schulman, Filip Wolski, Prafulla Dhariwal, Alec Radford, and Oleg Klimov. Proximal policy optimization algorithms, 2017. URL https://arxiv.org/abs/1707.06347.

Samuel L. Smith, Pieter-Jan Kindermans, Chris Ying, and Quoc V. Le. Don't decay the learning rate, increase the batch size. In *International Conference on Learning Representations (ICLR)*, 2018. URL https://openreview.net/forum?id=B1Yy1BxCZ.

Hwanjun Song, Minseok Kim, Dongmin Park, and Jae-Gil Lee. Learning from noisy labels: A survey. *ACM Computing Surveys*, 55(7):1–38, 2022. doi: 10.1145/3526242.

Tijmen Tieleman and Geoffrey Hinton. Lecture 6.5—rmsprop: Divide the gradient by a running average of its recent magnitude. COURSERA: Neural Networks for Machine Learning, 2012. Slides: http://www.cs.toronto.edu/~tijmen/csc321/slides/lecture_slides_lec6.pdf.

Emanuel Todorov, Tom Erez, and Yuval Tassa. Mujoco: A physics engine for model-based control. In *2012 IEEE/RSJ International Conference on Intelligent Robots and Systems*, pp. 5026–5033, 2012. doi: 10.1109/IROS.2012.6386109.

Mark Towers, Ariel Kwiatkowski, Jordan Terry, John U. Balis, Gianluca De Cola, Tristan Deleu, Manuel Goulão, Andreas Kallinteris, Markus Krimmel, Arjun KG, Rodrigo Perez-Vicente, Andrea Pierré, Sander Schulhoff, Jun Jet Tai, Hannah Tan, and Omar G. Younis. Gymnasium: A standard interface for reinforcement learning environments, 2024. URL https://arxiv.org/abs/2407.17032.

Alex Wang, Amanpreet Singh, Julian Michael, Felix Hill, Omer Levy, and Samuel R. Bowman. Glue: A multi-task benchmark and analysis platform for natural language understanding, 2019. URL https://arxiv.org/abs/1804.07461.

Jiayi Weng, Min Lin, Shengyi Huang, Bo Liu, Denys Makoviichuk, Viktor Makoviychuk, Zichen Liu, Yufan Song, Ting Luo, Yukun Jiang, Zhongwen Xu, and Shuicheng Yan. Envpool: A highly parallel reinforcement learning environment execution engine, 2022. URL https://arxiv.org/abs/2206.10558.

Xingyu Xie, Pan Zhou, Huan Li, Zhouchen Lin, and Shuicheng Yan. Adan: Adaptive nesterov momentum algorithm for faster optimizing deep models, 2024. URL https://arxiv.org/abs/2208.06677.

Sergey Zagoruyko and Nikos Komodakis. Wide residual networks, 2017. URL https://arxiv.org/abs/1605.07146.

Manzil Zaheer, Sashank J. Reddi, Devendra Sachan, Satyen Kale, and Sanjiv Kumar. Adaptive methods for nonconvex optimization. In *Advances in Neural Information Processing Systems 31*, pp. 9793–9803. Curran Associates, Inc., 2018. URL https://proceedings.neurips.cc/paper/2018/file/90365351ccc7437a1309dc64e4db32a3-Paper.pdf.

Matthew D. Zeiler. Adadelta: An adaptive learning rate method, 2012. URL https://arxiv.org/abs/1212.5701.

Chiyuan Zhang, Samy Bengio, Moritz Hardt, Benjamin Recht, and Oriol Vinyals. Understanding deep learning requires rethinking generalization. In *International Conference on Learning Representations (ICLR)*, 2017. URL https://openreview.net/forum?id=Sy8gdB9xx.

A ANOLOG PSEUDO CODE

Algorithm 2: Anolog without decoupled decay weights

Input: Initial parameters $x_1 \in \mathbb{R}^d$, learning rate η_k, decay rate $\beta_2 \in [0, 1)$, $\epsilon > 0$

Initialize $m_0 = 0$, $v_0 = 0$

for $k = 1$ **to** K **do**

Compute gradient $g_k = \nabla \ell(x_k)$

$\beta_1 = 1 - \frac{1}{\log(k+2)}$

$m_k = \beta_1 m_{k-1} + (1 - \beta_1) g_k$

$v_k = v_{k-1} - (1 - \beta_2) \cdot \text{sign}(v_{k-1} - g_k^2) \cdot g_k^2$

$x_{k+1} = x_k - \frac{\eta_k}{\sqrt{v_k + \epsilon}} \cdot |g_k| \cdot \text{sign}(m_k) - \eta_k \lambda x_k$

B HYPERPARAMETER TUNING PROTOCOL

To guarantee a balanced comparison, we carried out exhaustive grid searches on lightweight proxy tasks representative of each domain. The campaign comprised **2160** independent training runs, corresponding to 40 GPU-hours per optimiser. Adan introduces a third momentum coefficient; to keep the computational budget uniform we vary only (β_1, β_3), which govern the first and second moment estimates, respectively, while fixing the nesterov term at its default value $\beta_2 = 0.92$. For Anolog, we tuned the learning rate and the β_2 value.

Computer-vision proxy. Starting from CIFAR-10, we drew a balanced subset of 10,000 training images and 2,000 test images. We applied the identical augmentation pipeline used in Section 6 (random cropping, horizontal flips, and Cutout). Each hyperparameter configuration was trained for 20 epochs under five independent seeds with a ResNet-18 backbone. During training, we monitored validation accuracy and retained the single best accuracy per seed. Reported values are the mean and standard deviation of these maxima across seeds.

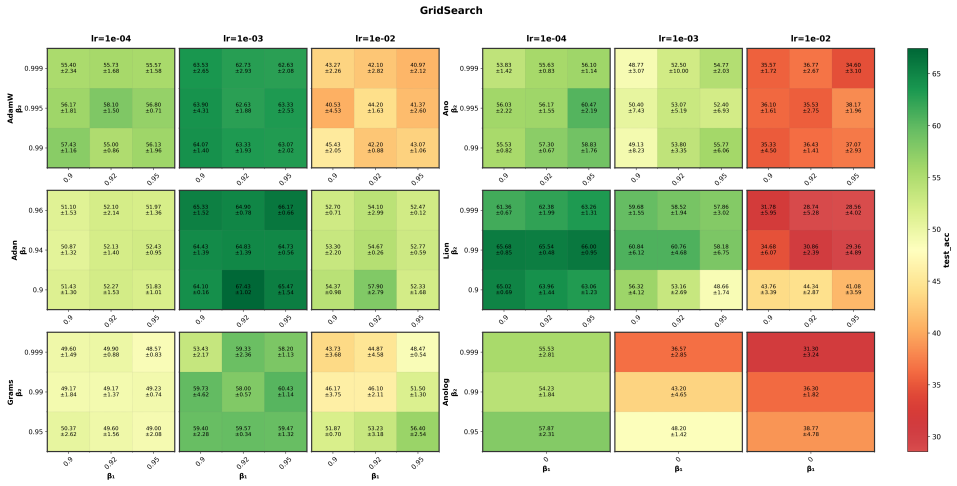

Figure 5: Validation-accuracy trajectories on the CIFAR-10 proxy (ResNet-18) for a representative subset of optimizers. Shaded areas denote ± 1 s.d. across five seeds.

For Adam, the best performance was achieved with a learning rate of $1\text{e}{-3}$. The optimizer showed low sensitivity to β values across the tested range; however, the configuration $\beta_1 = 0.9$, $\beta_2 = 0.99$ yielded the highest accuracy and lowest standard deviation across learning rates. This configuration was retained for subsequent experiments.

For Ano, optimal performance was obtained with a lower learning rate of $1\text{e}{-4}$, which is atypical for ResNet training. The best results corresponded to $\beta_1 = 0.95$ and $\beta_2 = 0.995$.

For Adan, the highest accuracy was observed at $\mathrm{lr} = 1\mathrm{e}{-3}$, with a strong synergy between $\beta_1 = 0.92$ and $\beta_2 = 0.9$ across all tested learning rates.

For Lion, optimal accuracy was reached with $\mathrm{lr} = 1\mathrm{e}{-4}$. While performance was largely insensitive to β_1, $\beta_2 = 0.99$ consistently produced the best results. We therefore selected $\beta_1 = 0.9$, $\beta_2 = 0.99$.

For Grams, the selected configuration was $\mathrm{lr} = 1\mathrm{e}{-3}$, $\beta_1 = 0.95$, and $\beta_2 = 0.99$ based on consistent high performance.

For Anolog, we adopted the same learning rate as for Ano ($1\mathrm{e}{-4}$), which yielded the best results. As β_2 had a notable impact across learning rates and values below the recommended threshold performed better, we fixed $\beta_2 = 0.95$.

NLP proxy. We fine-tune `BERT-base-uncased` on the MRPC paraphrase corpus for five epochs. MRPC's high label noise amplifies gradient variance, making the task an inexpensive yet sensitive probe of optimiser stability. A preliminary sweep showed that learning rates outside the range $[1\times10^{-5},\ 7\times10^{-5}]$ yield uniformly poor accuracies; subsequent grids therefore focus on a narrower band centred at 2×10^{-5}.

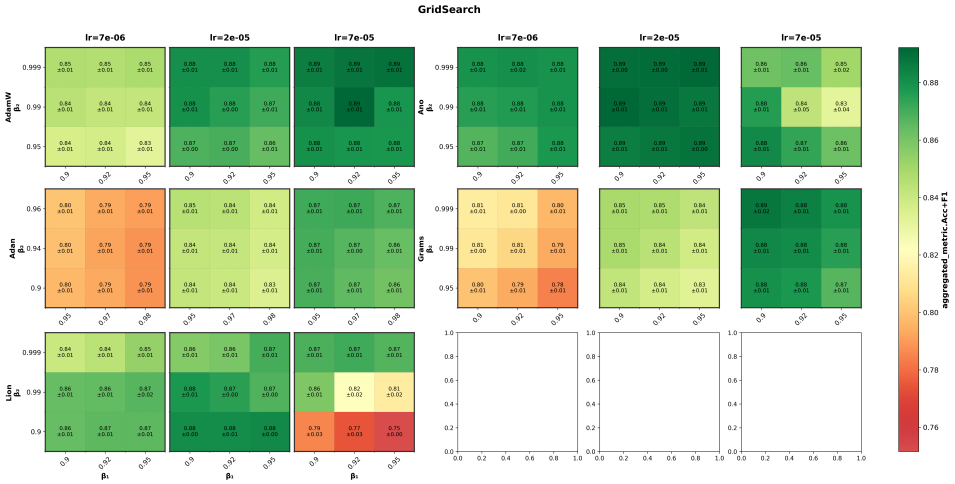

Figure 6: Grid-search results on MRPC used as an NLP proxy for hyper-parameter selection.

Adam achieves its highest validation performance at a learning rate of $\eta = 7 \times 10^{-5}$ and is only weakly sensitive to (β_1, β_2), with the standard configuration $(0.9, 0.999)$ remaining close to optimal.

Adan, in line with previous findings, favors larger learning rates, also peaking at $\eta = 7 \times 10^{-5}$. It displays strong sensitivity to β_1, with the best results obtained for $(\beta_1, \beta_2) = (0.95, 0.92)$ and a third momentum parameter $\beta_3 = 0.96$.

Ano shows minimal sensitivity to both learning rate and momentum parameters. Its optimal configuration is found at $\eta = 2 \times 10^{-5}$ with $(\beta_1, \beta_2) = (0.9, 0.999)$.

Lion reaches its best validation score at $\eta = 2 \times 10^{-5}$ and $\beta_2 = 0.9$. The choice of β_1 appears to have limited impact; we thus retain the standard $\beta_1 = 0.9$.

Grams performs best with a learning rate of $\eta = 7 \times 10^{-5}$ and the default $(\beta_1, \beta_2) = (0.9, 0.999)$ configuration.

Anolog yields its highest performance at $\eta = 2 \times 10^{-5}$, with $\beta_2 = 0.99$ proving consistently superior. As β_1 had negligible influence, we fix it to 0.9.

Deep-RL proxy. For Deep reinforcement learning, we adopted the MuJoCo HALFCHEETAH-V5 environment and capped training at 1×10^5 interaction steps, a budget that suffices to reveal optimisation speed without incurring prohibitive wall-clock cost. Agents were trained with the **Soft**

Actor–Critic (SAC) algorithm, and five seeds were run per hyperparameter setting. We report the final episodic return together with its standard deviation, and visualise learning curves in Fig. 7.

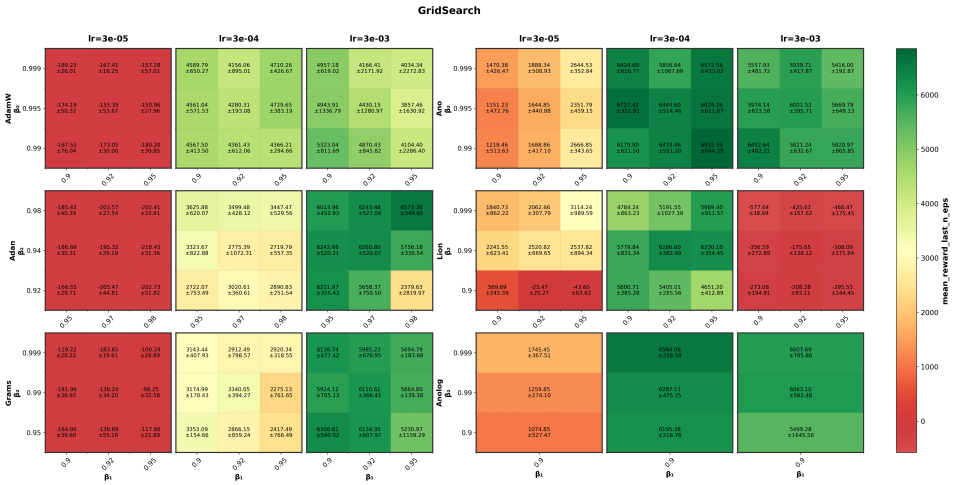

Figure 7: Learning curves on HALFCHEETAH-V5 using SAC. Curves show mean return; shading indicates ± 1 s.d. over seeds.

Figure 7 shows that while Adam appears to reach its peak performance at the relatively large step size $\eta = 3 \times 10^{-3}$, this result is likely overestimated due to the 100k-step evaluation window. Larger learning rates tend to accelerate early progress but stall quickly, resulting in higher variance. To ensure greater stability, we adopt the more conservative setting $\eta = 3 \times 10^{-4}$ with $(\beta_1, \beta_2) = (0.95, 0.995)$, which achieves comparable performance with significantly reduced variability.

Ano exhibits low sensitivity to the tested hyperparameter range. Nevertheless, the configuration $\eta = 3 \times 10^{-4}$ with $(\beta_1, \beta_2) = (0.95, 0.99)$ consistently yields the highest average score and is therefore selected.

For Adan, the best performance is obtained at $\eta = 3 \times 10^{-3}$ with $(\beta_1, \beta_2, \beta_3) = (0.98, 0.92, 0.98)$, consistent with the optimizer's preference for higher learning rates.

For Lion, the optimal configuration corresponds to $(\beta_1, \beta_2) = (0.92, 0.99)$.

Grams performs best with a more aggressive learning rate of $\eta = 3 \times 10^{-3}$ and momentum coefficients $(\beta_1, \beta_2) = (0.9, 0.95)$.

C CONVERGENCE PROOF FOR ANO

C.1 ALGORITHMIC UPDATE

For each coordinate $i \in [d]$ the optimizer maintains a first-order momentum $m_{k,i}$ and a second moment $v_{k,i}$ updated as in YOGI (Zaheer et al., 2018):

$$m_{k,i} = \beta_{1,k} m_{k-1,i} + (1 - \beta_{1,k}) g_{k,i}, \qquad v_{k,i} = v_{k-1,i} - (1 - \beta_2)\ \mathrm{sign}\big(v_{k-1,i} - g_{k,i}^2\big)\, g_{k,i}^2, \quad (1)$$

with $\beta_{1,k} = 1 - \frac{1}{\sqrt{k+1}}$ for $k \geq 1$; $\beta_2 \in (0, 1)$ and $m_{0,i} = v_{0,i} = 0$. The parameter vector is then updated by

$$x_{k+1,i} = x_{k,i} - \frac{\eta_k}{\sqrt{v_{k-1,i}} + \varepsilon} \, |g_{k,i}| \ \mathrm{sign}(m_{k,i}), \quad (2)$$

where $\varepsilon > 0$ is a fixed constant.

$$\eta_k = \frac{\eta}{(k+2)^{3/4}}, \qquad k = 0, 1, \ldots \quad (3)$$

All conditional expectations $\mathbb{E}_{k-1}[\,\cdot\,] = \mathbb{E}[\,\cdot\,|\mathcal{F}_{k-1}]$

C.2 STANDING ASSUMPTIONS

Assumption 1 (Smoothness). *The objective function $f : \mathbb{R}^d \to \mathbb{R}$ is differentiable and L-smooth; that is, for all $x, y \in \mathbb{R}^d$,*

$$\|\nabla f(x) - \nabla f(y)\| \le L\|x - y\|.$$

Assumption 2 (Lower boundedness). *The function f is bounded from below: there exists $f^\star > -\infty$ such that $f(x) \ge f^\star$ for all $x \in \mathbb{R}^d$.*

Assumption 3 (Bounded gradients). *There exists a constant $G > 0$ such that $\|\nabla f(x)\| \le G$ for all iterates x.*

Assumption 4 (Unbiased stochastic gradients). *At each iteration k, we observe a stochastic gradient $g_k \in \mathbb{R}^d$ satisfying $\mathbb{E}[g_{k,i} \mid \mathcal{F}_{k-1}] = \nabla_i f(x_k)$ for all $i \in [d]$.*

Assumption 5 (Bounded variance). *There exists $\sigma > 0$ such that for all $i \in [d]$ and $k \ge 1$,*

$$\mathbb{E}[(g_{k,i} - \nabla_i f(x_k))^2 \mid \mathcal{F}_{k-1}] \le \sigma^2.$$

C.3 AUXILIARY QUANTITIES

Define the two per-iteration scalars

$$A_k := \sum_{i=1}^{d} \frac{\nabla_i f(x_k)\,|g_{k,i}|\,\operatorname{sign}(m_{k,i})}{\sqrt{v_{k-1,i}} + \varepsilon}, \qquad B_k := \frac{L}{2} \sum_{i=1}^{d} \frac{g_{k,i}^2}{(\sqrt{v_{k-1,i}} + \varepsilon)^2}. \tag{4}$$

These two terms govern the decrease of the objective:

$$f(x_{k+1}) \le f(x_k) - \eta_k A_k + \eta_k^2 B_k. \tag{5}$$

C.4 LEMMA FOR PROBABILITY SIGN-MISMATCH

Lemma 1 (Sign-Mismatch Probability for Ano). *Fix any coordinate $i \in [d]$, under Assumptions 1–5 and following update rules equation 2-equation 1, with $\beta_{1,k} = 1 - \frac{1}{\sqrt{k+1}}$ and $\eta_k = (k+2)^{-3/4}$. Then for every $k \ge 1$,*

$$\mathbb{P}(\operatorname{sign}(m_{k,i}) \ne \operatorname{sign}(\nabla_i f(x_k)) \le \frac{C_m^2}{|\nabla_i f(x_k)|^2 \sqrt{k+1}}$$

with $C_m \coloneqq \sqrt{2(C_\Delta^2 + \sigma^2)}$ and $C_\Delta^2 = \frac{L^2 d(\sigma^2 + G^2)}{\varepsilon^2}$

Proof. We fix a coordinate $i \in [d]$. Define the per-coordinate momentum error as

$$e_{k,i} := m_{k,i} - \nabla_i f(x_k).$$

Subtracting $\nabla_i f(x_k)$ from the update rule of $m_{k,i}$ yields:

$$\begin{aligned} e_{k,i} &= \beta_{1,k} m_{k-1,i} + (1 - \beta_{1,k}) g_{k,i} - \nabla_i f(x_k) \\ &= \beta_{1,k}(m_{k-1,i} - \nabla_i f(x_{k-1})) + \beta_{1,k}(\nabla_i f(x_{k-1}) - \nabla_i f(x_k)) + (1 - \beta_{1,k})(g_{k,i} - \nabla_i f(x_k)) \end{aligned}$$

Define $\Delta_{k,i} := \nabla_i f(x_{k-1}) - \nabla_i f(x_k)$ as the gradient variation, and $\xi_{k,i} := g_{k,i} - \nabla_i f(x_k)$ as the stochastic noise for coordinate i.

$$e_{k,i} = \beta_{1,k} e_{k-1,i} + \beta_{1,k} \Delta_{k,i} + (1 - \beta_{1,k}) \xi_{k,i},$$

Conditionally on $\mathcal{F}_{k-1}$, define $V_{k,i} := \mathbb{E}_{k-1}[e_{k,i}^2]$:

$$V_{k,i} = \mathbb{E}_{k-1}\left[(\beta_{1,k} e_{k-1,i} + \beta_{1,k} \Delta_{k,i} + (1 - \beta_{1,k}) \xi_{k,i})^2\right].$$

Since $\mathbb{E}_{k-1}[\xi_{k,i}] = 0$ (Ass. 4), all mixed terms involving $\xi_{k,i}$ vanish after taking $\mathbb{E}_{k,i}$. Thus,

$$V_{k,i} = \mathbb{E}_{k-1}\left[(\beta_{1,k} e_{k-1,i} + \beta_{1,k} \Delta_{k,i})^2\right] + (1 - \beta_{1,k})^2 \mathbb{E}_{k-1}[\xi_{k,i}^2].$$

We now apply Young's inequality for scalars: $(a+b)^2 \leq (1+\delta)a^2 + (1+1/\delta)b^2$ for any $\delta > 0$. We set $\delta = \frac{1}{\sqrt{k+1}}$ (this minimizes the resulting upper bound). Applying this gives:

$$\mathbb{E}_{k-1}\left[(\beta_{1,k}e_{k-1,i} + \beta_{1,k}\Delta_{k,i})^2\right] \leq \left(1 + \frac{1}{\sqrt{k+1}}\right)\beta_{1,k}^2\mathbb{E}_{k-1}[e_{k-1,i}^2] + (1+\sqrt{k+1})\beta_{1,k}^2\mathbb{E}_{k-1}[\Delta_{k,i}^2].$$

Therefore,

$$V_{k,i} \leq \left(1 + \frac{1}{\sqrt{k+1}}\right)\beta_{1,k}^2 V_{k-1,i} + (1+\sqrt{k+1})\beta_{1,k}^2\mathbb{E}_{k-1}[\Delta_{k,i}^2] + (1-\beta_{1,k})^2\sigma^2.$$

To bound $\mathbb{E}_{k-1}[\Delta_{k,i}^2]$, we use the L-smoothness of f (Assumption 1). We have:

$$|\Delta_{k,i}| = |\nabla_i f(x_{k-1}) - \nabla_i f(x_k)| \leq \|\nabla f(x_{k-1}) - \nabla f(x_k)\|_2 \leq L\|x_k - x_{k-1}\|_2.$$

Hence,

$$\mathbb{E}_{k-1}[\Delta_{k,i}^2] \leq L^2\mathbb{E}_{k-1}[\|x_k - x_{k-1}\|_2^2].$$

Now we bound the step size:

$$\begin{aligned}
\mathbb{E}_{k-1}[\|x_k - x_{k-1}\|_2^2] &= \mathbb{E}_{k-1}\left[\sum_{j=1}^{d}\left(\frac{\eta_{k-1}}{\sqrt{v_{k-1,j}} + \varepsilon}|g_{k-1,j}|\right)^2\right] \\
&\leq \eta_{k-1}^2\sum_{j=1}^{d}\mathbb{E}_{k-1}\left[\frac{g_{k-1,j}^2}{\varepsilon^2}\right] \\
&\leq \frac{\eta_{k-1}^2}{\varepsilon^2}\sum_{j=1}^{d}\mathbb{E}_{k-1}[g_{k-1,j}^2].
\end{aligned}$$

By Assumptions 3-5, we have $\mathbb{E}_{k-1}[g_{k-1,j}^2] \leq \sigma^2 + G^2$, where σ^2 is the variance bound and G is an upper bound on the gradient norm. Thus,

$$\mathbb{E}_{k-1}[\|x_k - x_{k-1}\|_2^2] \leq \frac{d\eta_{k-1}^2(\sigma^2 + G^2)}{\varepsilon^2}.$$

Let $C_\Delta^2 := \frac{L^2 d(\sigma^2+G^2)}{\varepsilon^2}$. Then, we obtain:

$$\mathbb{E}_{k-1}[\Delta_{k,i}^2] \leq C_\Delta^2\eta_{k-1}^2.$$

Putting everything together, we get the recurrence:

$$V_{k,i} \leq \left(1 + \frac{1}{\sqrt{k+1}}\right)\beta_{1,k}^2 V_{k-1,i} + (1+\sqrt{k+1})\beta_{1,k}^2 C_\Delta^2\eta_{k-1}^2 + (1-\beta_{1,k})^2\sigma^2.$$

Set $\beta_{1,k} = 1 - \frac{1}{\sqrt{k+1}}$ and $\eta_k = 1/(k+1)^{3/4}$, to simplify we denote $l = k+1$.

$$\begin{aligned}
V_{k,i} &\leq (1 + \frac{1}{\sqrt{l}})(1 - \frac{1}{\sqrt{l}})^2 V_{k-1,i} + (1+\sqrt{l})(1-\frac{1}{\sqrt{l}})^2 C_\Delta^2\frac{1}{l^{3/2}} + \frac{\sigma^2}{k+1} \\
V_{k,i} &\leq (1 - \frac{1}{\sqrt{l}} - \frac{1}{l} + \frac{1}{l^{3/2}})V_{k-1,i} + \frac{1}{l}\left[(1+\frac{1}{\sqrt{l}})(1-\frac{1}{\sqrt{l}})^2 C_\Delta^2 + \sigma^2\right]
\end{aligned}$$

Hence $a_k := (1 - \frac{1}{\sqrt{l}} - \frac{1}{l} + \frac{1}{l^{3/2}})$ and $B_k := \frac{1}{l}\left[(1+\frac{1}{\sqrt{l}})(1-\frac{1}{\sqrt{l}})^2 C_\Delta^2 + \sigma^2\right]$, with $a_k \leq 1 - \frac{1}{\sqrt{l}}$ and $B_k = \mathcal{O}(l^{-1})$.So, we can express the inequality on this way

$$V_{k,i} \leq a_k V_{k-1,i} + B_k$$

Simplifying the coefficients. For $k \geq 1$,

$$a_k \;=\; 1 - \frac{1}{\sqrt{l}} - \frac{1}{l} + \frac{1}{l^{3/2}} \;\leq\; 1 - \frac{1}{\sqrt{l}}, \qquad (1 + l^{-1/2})(1 - l^{-1/2})^2 \;\leq\; 1,$$

so that

$$a_k \leq 1 - \frac{1}{\sqrt{l}}, \qquad B_k \leq \frac{C_B}{l}, \quad C_B := C_\Delta^2 + \sigma^2. \tag{6}$$

We want to simplify this bound by having a bound with the form $V_{k,i} \leq \mathcal{O}\left(\frac{1}{\sqrt{l}}\right)$, to proceed, we will prove by induction that $V_{k,i} = O(1/\sqrt{l})$. Specifically, we posit that there exists a constant M such that for all sufficiently large k, $V_{k,i} \leq \frac{M}{\sqrt{l}}$.

Base Case We can choose M large enough such that the hypothesis holds for some initial $k_0 \geq 1$.

Inductive Step Assume that for some $k > k_0$, the hypothesis $V_{k-1} \leq \frac{M}{\sqrt{k-1}}$ holds. We must show that $V_{k,i} \leq \frac{M}{\sqrt{l}}$. From our simplified recurrence, we have:

$$V_{k,i} \leq \left(1 - \frac{1}{\sqrt{l}}\right) \frac{M}{\sqrt{l-1}} + \frac{C_B}{l}$$

The induction holds if we can prove:

$$\left(1 - \frac{1}{\sqrt{l}}\right) \frac{M}{\sqrt{l-1}} + \frac{C_B}{l} \leq \frac{M}{\sqrt{l}}$$

Rearranging the terms, this is equivalent to showing:

$$\frac{C_B}{l} \leq M\left(\frac{1}{\sqrt{l}} - \frac{1}{\sqrt{l-1}} + \frac{1}{\sqrt{l}\sqrt{l-1}}\right)$$

To analyze the right-hand side (RHS) for large k, we use a Taylor expansion for the term $(l-1)^{-1/2}$:

$$\frac{1}{\sqrt{l-1}} = (l-1)^{-1/2} = l^{-1/2}\left(1 - \frac{1}{l}\right)^{-1/2}$$

Using the expansion $(1-x)^{-1/2} = 1 + \frac{x}{2} + O(x^2)$, we get:

$$\frac{1}{\sqrt{l-1}} = \frac{1}{\sqrt{l}}\left(1 + \frac{1}{2l} + O\left(\frac{1}{l^2}\right)\right) = \frac{1}{\sqrt{l}} + \frac{1}{2l^{3/2}} + O\left(\frac{1}{l^{5/2}}\right)$$

Substituting this into the parenthesis on the RHS of our inequality, the term becomes:

$$\begin{aligned}
&\frac{1}{\sqrt{l}} - \left(\frac{1}{\sqrt{l}} + \frac{1}{2l^{3/2}}\right) + \frac{1}{l\sqrt{1-1/l}} + O\left(\frac{1}{l^{5/2}}\right) \\
=& -\frac{1}{2l^{3/2}} + \frac{1}{l}\left(1 + \frac{1}{2l} + O\left(\frac{1}{l^2}\right)\right) + O\left(\frac{1}{l^{5/2}}\right) \\
=& \frac{1}{l} - \frac{1}{2l^{3/2}} + O\left(\frac{1}{l^2}\right)
\end{aligned}$$

The full inequality we need to satisfy is therefore:

$$\frac{C_B}{l} \leq M\left(\frac{1}{l} - \frac{1}{2l^{3/2}} + O\left(\frac{1}{l^2}\right)\right)$$

Multiplying through by l, the condition becomes:

$$C_B \leq M\left(1 - \frac{1}{2\sqrt{l}} + O\left(\frac{1}{l}\right)\right)$$

This inequality shows why the induction works. For any choice of constant $M > C_B$, we can find a sufficiently large k_0 such that for all $k \geq k_0$, the inequality holds. This completes the induction,

establishing that $V_{k,i} \leq \frac{M}{\sqrt{l}}$. So, for a sufficiently large k_0 such that for all $k \geq k_0$, we have :

$$V_{k,i} \leq \frac{2C_B}{\sqrt{l}}$$
$$\mathbb{E}_{k-1}[(m_{k,i} - \nabla_i f(x_k))^2] \leq \frac{2(C_\Delta^2 + \sigma^2)}{\sqrt{l}}$$
$$\mathbb{E}_{k-1}[|m_{k,i} - \nabla_i f(x_k)|^2] \leq \frac{2(C_\Delta^2 + \sigma^2)}{\sqrt{l}}$$

We recall that $l = k + 1$, so

$$\mathbb{E}_{k-1}[|m_{k,i} - \nabla_i f(x_k)|^2] \leq \frac{2(C_\Delta^2 + \sigma^2)}{\sqrt{k+1}}$$

From moment bound to probability bound We bound the probability of a momentum–gradient sign mismatch. If $\text{sign}(m_{k,i}) \neq \text{sign}(\nabla_i f(x_k))$ and $\nabla_i f(x_k) \neq 0$, then $|m_{k,i} - \nabla_i f(x_k)| \geq |\nabla_i f(x_k)|$. Hence, for any $k \geq 1$,

$$\mathbb{P}_{k-1}\big(\text{sign}(m_{k,i}) \neq \text{sign}(\nabla_i f(x_k))\big) \leq \mathbb{P}\big(|m_{k,i} - \nabla_i f(x_k)| \geq |\nabla_i f(x_k)|\big)$$

We apply Chebyshev's inequality to the right-hand side:

$$\mathbb{P}_{k-1}\big(|m_{k,i} - \nabla_i f(x_k)| \geq |\nabla_i f(x_k)|\big) \leq \frac{\mathbb{E}_{k-1}\big[|m_{k,i} - \nabla_i f(x_k)|^2\big]}{|\nabla_i f(x_k)|^2}$$

Using the previously established second-moment bound, $\mathbb{E}_{k-1}[|m_{k,i} - \nabla_i f(x_k)|^2] \leq \frac{2(C_\Delta^2+\sigma^2)}{\sqrt{k+1}}$:

$$\mathbb{P}_{k-1}\big(\text{sign}(m_{k,i}) \neq \text{sign}(\nabla_i f(x_k))\big) \leq \frac{C_m^2}{|\nabla_i f(x_k)|^2\sqrt{k+1}}$$

with $C_m = \sqrt{2(C_\Delta^2 + \sigma^2)}$ □

C.5 Bound on A

Lemma 2 (Lower bound on the expected update magnitude)**.** *Assume all the condition (cf C.2. Recall*

$$A_k \;=\; \sum_{i=1}^{d} \frac{\nabla_i f(x_k)\,|g_{k,i}|\,\text{sign}(m_{k,i})}{\sqrt{v_{k-1,i}} + \varepsilon}, \qquad \mathbb{E}_{k-1}[\cdot] \;=\; \mathbb{E}[\cdot \mid \mathcal{F}_{k-1}].$$

Let

$$C_m = \sqrt{2(C_\Delta^2 + \sigma^2)}, \quad C_v = \frac{2d\sqrt{\sigma^2 + G^2}}{\varepsilon}$$

Then, for every iteration $k \geq k_0$,

$$\mathbb{E}[A_k] \geq \frac{\mathbb{E}[\|\nabla f(x_k)\|_2^2]}{\sqrt{2}G + \varepsilon} - \frac{C_v C_m}{(k+1)^{1/4}},$$

Proof. We begin by recalling the definition of A_k and factoring out constants that do not depend on $g_{k,i}$:

$$\mathbb{E}_{k-1}[A_k] = \sum_{i=1}^{d} \frac{\nabla_i f(x_k)}{\sqrt{v_{k-1,i}} + \varepsilon} \cdot \mathbb{E}_{k-1}\big[|g_{k,i}|\,\text{sign}(m_{k,i})\big].$$

Our goal is to lower bound the term $\mathbb{E}_{k-1}\big[|g_{k,i}|\,\text{sign}(m_{k,i})\big]$.

We first expand this term using the identity:

$$\text{sign}(m_{k,i}) = \text{sign}(\nabla_i f(x_k)) \cdot (1 - 2 \cdot \mathbb{I}\left[\text{sign}(\nabla_i f(x_k)) \neq \text{sign}(m_{k,i})\right]),$$

Let $\chi_{k,i} := \mathbb{I}\left[\text{sign}(\nabla_i f(x_k)) \neq \text{sign}(m_{k,i})\right]$. , we get:

$$\begin{aligned}\mathbb{E}_{k-1}\left[|g_{k,i}|\,\text{sign}(m_{k,i})\right] = \text{sign}(\nabla_i f(x_k)) \cdot \mathbb{E}_{k-1}\left[|g_{k,i}|\right] \\ - 2 \cdot \mathbb{E}_{k-1}\left[|g_{k,i}| \cdot \text{sign}(\nabla_i f(x_k)) \cdot \chi_{k,i}\right]\end{aligned}$$

where the second line follows from linearity of expectation.

We now bound the first term using Jensen

$$\text{sign}(\nabla_i f(x_k)) \cdot \mathbb{E}_{k-1}[|g_{k,i}|] \geq \text{sign}(\nabla_i f(x_k)) \cdot |\mathbb{E}_{k-1}[g_{k,i}]| = \nabla_i f(x_k),$$

where we used the assumption that $\mathbb{E}_{k-1}[g_{k,i}] = \nabla_i f(x_k)$.

We bound the second term by combining $\text{sign}(\nabla_i f(x_k)) \leq 1$ and Cauchy-Schwarz:

$$\mathbb{E}_{k-1}\left[|g_{k,i}| \cdot \text{sign}(\nabla_i f(x_k)) \cdot \chi_{k,i}\right] \leq \sqrt{\mathbb{E}_{k-1}\left[g_{k,i}^2\right]} \cdot \sqrt{\mathbb{E}_{k-1}\left[\chi_{k,i}^2\right]}$$

By the variance definition, we know that $\text{Var}(X) = \mathbb{E}[X^2] - (\mathbb{E}[X])^2$, so we have

$$\mathbb{E}_{k-1}\left[g_{k,i}^2\right] = \text{Var}_{k-1}(g_{k,i}) + \left(\mathbb{E}_{k-1}[g_{k,i}]\right)^2$$

By combining Assumptions (4, 3 and 5), and $\chi_{k,i}^2 = \chi_{k,i}$, we got :

$$\mathbb{E}_{k-1}\left[|g_{k,i}| \cdot \text{sign}(\nabla_i f(x_k)) \cdot \chi_{k,i}\right] \leq \sqrt{\sigma^2 + G^2} \cdot \sqrt{\mathbb{P}_{k-1}\left(\chi_{k,i}\right)}$$

By using lemma 1,

$$\mathbb{E}_{k-1}\left[|g_{k,i}| \cdot \text{sign}(\nabla_i f(x_k)) \cdot \chi_{k,i}\right] \leq \sqrt{\sigma^2 + G^2} \cdot \frac{C_m}{|\nabla_i f(x_k)|(k+1)^{1/4}}$$

We have so :

$$\mathbb{E}_{k-1}\left[|g_{k,i}|\,\text{sign}(m_{k,i})\right] \geq \nabla_i f(x_k) - 2 \cdot \sqrt{\sigma^2 + G^2} \cdot \frac{C_m}{|\nabla_i f(x_k)|(k+1)^{1/4}}$$

In our main equation, we have then

$$\mathbb{E}_{k-1}[A_k] \geq \sum_{i=1}^{d} \frac{\nabla_i f(x_k)}{\sqrt{v_{k-1,i}} + \varepsilon} \cdot \left(\nabla_i f(x_k) - 2 \cdot \sqrt{\sigma^2 + G^2} \cdot \frac{C_m}{|\nabla_i f(x_k)|(k+1)^{1/4}}\right)$$

$$\mathbb{E}_{k-1}[A_k] \geq \sum_{i=1}^{d} \frac{(\nabla_i f(x_k))^2}{\sqrt{v_{k-1,i}} + \varepsilon} - \frac{1}{(k+1)^{1/4}} \cdot 2\sqrt{\sigma^2 + G^2}\, C_m \sum_{i=1}^{d} \frac{1}{\sqrt{v_{k-1,i}} + \varepsilon}$$

Using the bound $0 \leq v_{k-1,i} \leq 2G^2$, which holds under the assumptions of Zaheer et al. (2018) (see Theorem 2), we deduce:

$$\mathbb{E}_{k-1}[A_k] \geq \frac{\|\nabla f(x_k)\|_2^2}{\sqrt{2}G + \varepsilon} - \frac{1}{(k+1)^{1/4}} \cdot \frac{2d\sqrt{\sigma^2 + G^2}\, C_m}{\varepsilon}$$

Finally, letting $C_v = \frac{2d\sqrt{\sigma^2+G^2}}{\varepsilon}$, we can write:

$$\mathbb{E}_{k-1}[A_k] \geq \frac{\|\nabla f(x_k)\|_2^2}{\sqrt{2}G + \varepsilon} - \frac{C_v C_m}{(k+1)^{1/4}},$$

By the total expectation law

$$\mathbb{E}[A_k] \geq \frac{\mathbb{E}[\|\nabla f(x_k)\|_2^2]}{\sqrt{2}G + \varepsilon} - \frac{C_v C_m}{(k+1)^{1/4}},$$

which concludes the proof. □

C.6 BOUND ON B

Lemma 3. *Assume the standing hypotheses of the paper hold, in particular (Assumptions 3-5)* $\mathbb{E}_{k-1}[g_{k,i}^2] \leq G^2 + \sigma^2$*, for all time-steps* k *and coordinates* i*, and let* $\varepsilon > 0$*. Then, for every iteration* $k \geq 1$*,*

$$\mathbb{E}[B_k] \leq \frac{L\, d\, (G^2 + \sigma^2)}{2\, \varepsilon^2}$$

Proof. Because $v_{k-1,i} \geq 0$ and $\varepsilon > 0$, we have

$$(\sqrt{v_{k-1,i}} + \varepsilon)^2 \;\geq\; \varepsilon^2.$$

Together with the bound $\mathbb{E}_{k-1}[g_{k,i}^2] \leq G^2 + \sigma^2$, this implies

$$\mathbb{E}_{k-1}\left[\frac{g_{k,i}^2}{(\sqrt{v_{k-1,i}} + \varepsilon)^2}\right] \;\leq\; \frac{G^2 + \sigma^2}{\varepsilon^2} \quad \text{for all } i.$$

Summing over $i = 1, \ldots, d$ and factoring out $L/2$ yields

$$\mathbb{E}_{k-1}[B_k] \;\leq\; \frac{L}{2}\, d\, \frac{(G^2 + \sigma^2)}{\varepsilon^2} = \frac{L\, d\, (G^2 + \sigma^2)}{2\, \varepsilon^2},$$

By the total expectation law

$$\mathbb{E}[B_k] \;\leq\; \frac{L\, d\, (G^2 + \sigma^2)}{2\, \varepsilon^2}$$

which completes the proof. □

C.7 MAIN RESULT

Theorem 1 (Convergence to a stationary point)**.** *Let Assumption C.2 hold and set the learning rate as in equation 3. Then for any horizon* $K \geq 1$*,*

$$\min_{0 \leq k < K} \mathbb{E}\big[\|\nabla f(x_k)\|_2^2\big] \leq \mathcal{O}\left(\frac{\log K}{K^{1/4}}\right).$$

Proof. The proof starts from the descent guarantee provided by the L-smoothness of $f(x)$, as stated in Equation equation 5:

$$f(x_{k+1}) \leq f(x_k) - \eta_k A_k + \eta_k^2 B_k.$$

Taking $\mathbb{E}_{k-1}$, we get:

$$\mathbb{E}[f(x_{k+1})] \leq \mathbb{E}[f(x_k)] - \eta_k \mathbb{E}[A_k] + \eta_k^2 \mathbb{E}[B_k].$$

We now bound the terms $\mathbb{E}[A_k]$ and $\mathbb{E}[B_k]$ using the provided lemmas.

1. **Bounding** $\mathbb{E}[A_k]$: From Lemma 2, we have:

$$\mathbb{E}[A_k] \geq \frac{1}{\sqrt{2}\, G + \varepsilon} \mathbb{E}[\|\nabla f(x_k)\|_2^2] - \frac{C_m C_v}{(k+1)^{\frac{1}{4}}}$$

2. **Bounding** $\mathbb{E}[B_k]$: From Lemma 3, B_k is uniformly bounded. Define $C_b := \frac{L\, d\, (G^2 + \sigma^2)}{2\, \varepsilon^2}$, then:

$$\mathbb{E}[B_k] \leq C_b.$$

Substituting into the main inequality:

$$\mathbb{E}[f(x_{k+1})] \leq \mathbb{E}[f(x_k)] - \frac{\eta_k}{\sqrt{2}\, G + \varepsilon} \mathbb{E}\big[\|\nabla f(x_k)\|_2^2\big] + \eta_k \frac{C_m C_v}{k^{1/4}} + \eta_k^2 C_b.$$

Let $\eta_k = \frac{\eta}{(k+2)^{3/4}} \leq \frac{\eta}{(k+1)^{3/4}}$. Then:

$$\mathbb{E}[f(x_{k+1})] \leq \mathbb{E}[f(x_k)] - \frac{\eta}{(k+1)^{3/4}(\sqrt{2}\,G+\varepsilon)}\mathbb{E}\big[\|\nabla f(x_k)\|_2^2\big] + \frac{C_m C_v \eta}{k+1} + \frac{\eta^2\, C_b}{(k+1)^{3/2}}$$

Rewriting:

$$\frac{\eta}{(k+1)^{3/4}(\sqrt{2}\,G+\varepsilon)}\mathbb{E}\big[\|\nabla f(x_k)\|_2^2\big] \leq \mathbb{E}[f(x_k)] - \mathbb{E}[f(x_{k+1})] + \frac{C_m C_v \eta}{k+1} + \frac{\eta^2\, C_b}{(k+1)^{3/2}}$$

Summing from $k = 0$ to $K-1$:

$$\sum_{k=0}^{K-1} \frac{\eta}{(k+1)^{3/4}(\sqrt{2}\,G+\varepsilon)}\mathbb{E}\big[\|\nabla f(x_k)\|_2^2\big] \leq f(x_0) - f^\star + C_m C_v \eta \sum_{k=0}^{K-1} \frac{1}{k+1} + \eta^2\, C_b \sum_{k=0}^{K-1} \frac{1}{(k+1)^{3/2}}$$

The harmonic sum satisfies:

$$\sum_{k=0}^{K-1} \frac{1}{k+1} \leq 1 + \log K.$$

The second term is a convergent p-series with exponent $p = 3/2 > 1$; hence it converges to a finite limit as $K \to \infty$. Therefore, the partial sum can be bounded by the value of the full series:

$$\eta^2\, C_b \sum_{k=0}^{K-1} (k+1)^{-3/2} \;\leq\; \eta^2\, C_b \sum_{k=0}^{\infty} k^{-3/2} \;=\; \eta^2\, C_b\, \zeta\big(\tfrac{3}{2}\big) \;=: C_R,$$

where $\zeta(\cdot)$ denotes the Riemann zeta function. We thus define the constant $C_R := \eta^2 C_b \zeta\big(\frac{3}{2}\big)$.

By combining these terms, we have for the main equation:

$$\sum_{k=0}^{K-1} \frac{1}{(k+1)^{3/4}}\mathbb{E}\big[\|\nabla f(x_k)\|_2^2\big] \leq \frac{1}{C_{LHS}}\left[f(x_0) - f^\star + C_{sum}(1+\log K) + C_R\right]$$

with $C_{sum} = C_m C_v \eta$ and $C_{LHS} = \frac{\eta}{\sqrt{2}G+\epsilon}$.

The left-hand side can be lower-bounded as follows:

$$\sum_{k=1}^{K-1} \frac{1}{(k+1)^{3/4}}\mathbb{E}\big[\|\nabla f(x_k)\|_2^2\big] \geq \min_{0\leq k<K} \mathbb{E}\big[\|\nabla f(x_k)\|_2^2\big] \sum_{k=1}^{K-1} \frac{1}{(k+1)^{3/4}}$$

Now, let's find a lower bound for the sum. We can approximate it with an integral:

$$\sum_{k=0}^{K-1} \frac{1}{(k+1)^{3/4}} = \sum_{j=1}^{K} \frac{1}{j^{3/4}} \geq \int_1^{K+1} \frac{1}{x^{3/4}} dx = \Big[4x^{1/4}\Big]_1^{K+1} = 4\left((K+1)^{1/4} - 1\right)$$

For a large K, this sum is of the order $\mathcal{O}(K^{1/4})$.

Substituting this back into our main inequality, we get:

$$4\left((K+1)^{1/4} - 1\right) \min_{0\leq k<K} \mathbb{E}\big[\|\nabla f(x_k)\|_2^2\big] \leq \frac{1}{C_{LHS}}\left[f(x_0) - f^\star + C_{sum}(1+\log K) + C_R\right]$$

Now, we can isolate the minimum of the expected squared norm of the gradient:

$$\min_{0\leq k<K} \mathbb{E}\big[\|\nabla f(x_k)\|_2^2\big] \leq \frac{f(x_0) - f^\star + C_{sum}(1+\log K) + C_R}{4C_{LHS}\left((K+1)^{1/4} - 1\right)}$$

As $K \to \infty$, the dominant terms are $\log K$ in the numerator and $K^{1/4}$ in the denominator. Therefore, we can write the convergence rate as:

$$\min_{0\leq k<K} \mathbb{E}\big[\|\nabla f(x_k)\|_2^2\big] = \mathcal{O}\left(\frac{\log K}{K^{1/4}}\right) = \tilde{\mathcal{O}}\left(\frac{1}{K^{1/4}}\right)$$

Remark 1 (On the choice of hyperparameters)**.** *The convergence analysis required carefully tuned hyperparameters. In particular, we employed a progressively increasing momentum coefficient, $\beta_{1,k} = 1 - 1/\sqrt{k}$, along with a relatively aggressive learning rate schedule. This combination was essential to control key residual terms throughout the proof and to ensure overall convergence. While more conservative choices failed to yield meaningful bounds, the schedule used here proved sufficient for our theoretical guarantees.*

Remark 2 (On the convergence rate)**.** *The convergence rate $\mathcal{O}(\log K/K^{1/4})$ for $\min_k \mathbb{E}[\|\nabla f(x_k)\|^2]$ arises intrinsically from the sign-based nature of the update rule. Unlike gradient-magnitude-based methods, our approach relies solely on the sign of momentum terms, which demands high directional accuracy. Ensuring this accuracy requires a tight control over the momentum error variance, which in turn necessitates a fast-decaying learning rate, $\eta_k = \mathcal{O}(k^{-3/4})$. This schedule guarantees reliable update directions but slows the overall convergence, as the learning rate bounds the algorithm's progress. Hence, the rate reflects a fundamental trade-off: stability of sign-based directions versus the speed of descent.*

□

D Additional Results

D.1 Full Results on Analysis Parts

Optimizer	$\sigma = 0$	0.01	0.05	0.10	0.20
Ano	82.25 ± 0.09	78.78 ± 0.24	71.0 ± 0.33	65.96 ± 0.15	59.81 ± 0.74
Adam	80.89 ± 0.29	76.08 ± 0.3	66.43 ± 0.08	60.56 ± 0.37	53.01 ± 0.86
Lion	81.23 ± 0.24	77.69 ± 0.15	69.40 ± 0.11	64.03 ± 0.93	57.07 ± 0.94
Grams	71.37 ± 0.33	77.91 ± 0.03	70.56 ± 0.23	65.47 ± 0.32	58.8 ± 0.58

Table 7: CIFAR-10 test accuracy (%) $\pm$ std.

D.2 Full Normalized Score for SAC

Optimizers	HalfCheetah-v5 Score±IC	Norm	Ant-v5 Score±IC	Norm	Humanoid-v5 Score±IC	Norm	Walker2d-v5 Score±IC	Norm	Hopper-v5 Score±IC	Norm	Avg. Norm
Baseline											
Adam	9477.97 ± 1003.20	87.34	4161.08 ± 515.06	79.30	$\mathbf{5247.63 \pm 105.87}$	**100**	4276.75 ± 238.68	83.55	2922.12 ± 284.42	99.85	90.01
Adan	8796.97 ± 955.18	81.06	3294.58 ± 433.50	62.79	5116.14 ± 125.19	97.49	3698.10 ± 572.68	72.24	2509.11 ± 324.34	85.74	79.87
Lion	7406.13 ± 2772.84	68.25	3491.82 ± 579.52	66.55	85.58 ± 28.33	1.63	4768.21 ± 201.84	93.15	703.34 ± 657.37	24.03	50.72
Grams	6457.31 ± 879.37	59.50	3031.85 ± 478.99	57.78	5181.55 ± 105.09	98.74	3386.75 ± 896.29	66.16	2606.07 ± 579.75	89.05	74.25
Ano (Ours)	$\mathbf{10851.80 \pm 518.67}$	**100**	$\mathbf{5247.02 \pm 653.98}$	**100**	5190.86 ± 136.30	98.92	$\mathbf{5119.08 \pm 420.88}$	**100**	$\mathbf{2926.39 \pm 308.72}$	**100**	**99.78**
Anolog (Ours)	10389.50 ± 1041.29	95.74	4598.67 ± 727.16	87.64	5161.95 ± 268.91	98.37	4748.18 ± 593.57	92.75	2585.67 ± 238.48	88.36	92.57
Tuned											
Adam	9874.24 ± 735.62	87.67	4110.11 ± 692.96	76.26	$\mathbf{5308.70 \pm 195.70}$	**100**	4369.92 ± 326.27	87.73	$\mathbf{3143.48 \pm 233.52}$	**100**	90.33
Adan	10133.64 ± 849.35	89.97	5222.12 ± 218.59	96.90	5034.40 ± 95.83	94.83	$\mathbf{4981.25 \pm 184.94}$	**100**	2971.66 ± 367.72	94.53	95.25
Lion	7351.97 ± 3058.09	65.27	2826.41 ± 1698.65	52.44	86.81 ± 24.43	1.64	4496.17 ± 519.54	90.26	430.78 ± 260.73	13.70	44.66
Grams	8522.14 ± 1648.23	75.66	4187.69 ± 707.71	77.70	5116.82 ± 135.39	96.39	4204.40 ± 836.06	84.40	2870.06 ± 740.79	91.30	85.09
Ano (Ours)	$\mathbf{11263.08 \pm 284.18}$	**100**	$\mathbf{5389.34 \pm 353.92}$	**100**	5071.59 ± 138.17	95.53	4810.42 ± 356.80	96.57	2972.84 ± 418.39	94.57	**97.34**

Table 8: Comparison of the average performance (± IC95%) and normalized scores of different optimizers across MuJoCo environments.

D.3 Full Normalized Score for PPO

E Hyperparameters Settings

E.1 Optimizers Hyperparameters

Optimizers	BattleZone-v5 Score±IC	Norm	DoubleDunk-v5 Score±IC	Norm	NameThisGame-v5 Score±IC	Norm	Phoenix-v5 Score±IC	Norm	Qbert-v5 Score±IC	Norm	Avg. Norm
Baseline											
Adam	7656.00 ± 812.20	91.19	**−0.91 ± 0.34**	**100**	733.92 ± 107.34	90.99	**3516.64 ± 475.14**	**100**	4322.00 ± 254.93	79.83	92.40
Adan	6408.00 ± 1525.14	76.32	−0.98 ± 0.21	99.58	633.80 ± 44.93	78.58	2033.76 ± 85.42	57.83	2100.60 ± 951.20	38.80	70.22
Lion	1420.00 ± 256.88	16.91	−1.96 ± 1.50	93.84	564.44 ± 195.39	69.98	2477.12 ± 490.65	70.44	3680.80 ± 1057.34	67.99	63.83
Grams	**8396.00 ± 1565.13**	**100**	−1.07 ± 0.55	99.09	644.64 ± 48.73	79.92	2133.76 ± 234.64	60.68	3646.70 ± 1139.41	67.36	81.41
Ano (Ours)	8280.00 ± 916.31	98.62	−1.03 ± 0.21	99.30	**806.56 ± 114.49**	**100**	2808.68 ± 465.32	79.87	5122.12 ± 783.72	94.61	**94.48**
Anolog (Ours)	7620.00 ± 1225.14	90.76	−1.07 ± 0.26	99.08	743.00 ± 191.30	92.12	2815.50 ± 430.55	80.06	**5413.75 ± 1873.65**	**100**	92.40
Tuned											
Adam	7880.00 ± 1218.48	82.46	**−0.93 ± 0.15**	**100**	663.87 ± 178.56	90.45	2964.16 ± 601.40	98.14	4222.90 ± 256.83	81.50	90.51
Adan	4672.00 ± 2542.63	48.89	−1.08 ± 0.27	99.11	693.96 ± 87.13	94.55	**3020.48 ± 419.22**	**100**	4540.20 ± 996.34	87.62	86.03
Lion	1296.00 ± 164.16	13.56	−2.73 ± 1.92	89.46	550.96 ± 134.29	75.07	2554.80 ± 546.74	84.58	3267.00 ± 915.37	63.05	65.14
Grams	7536.00 ± 240.38	78.86	−1.41 ± 0.46	97.19	704.68 ± 123.61	96.01	1864.92 ± 204.72	61.74	4962.38 ± 1373.46	95.77	85.91
Ano (Ours)	**9556.00 ± 2370.99**	**100**	−1.13 ± 0.43	98.83	**733.95 ± 235.51**	**100**	2862.24 ± 365.46	94.76	**5181.70 ± 1210.60**	**100**	**98.72**

Table 9: Comparison of the average performance (± IC95%) and normalized scores of different optimizers across Atari environments.

Table 10: Optimizers hyperparameter settings used in all experiments.

Model	**Optimizer**	β_1	β_2	β_3	lr	λ
Noise Robustness Analysis						
CNN	AdamW	0.9	0.999	–	1e-3	–
	Lion	0.9	0.99	–	1e-4	–
	Ano	0.92	0.99	–	1e-4	–
	Grams	0.9	0.999	–	1e-3	–
Computer Vision (CIFAR-100)						
Baseline						
ResNet-34	AdamW	0.9	0.999	–	1e-3	1e-2
	Adan	0.98	0.92	0.99	1e-3	1e-2
	Ano	0.92	0.99	–	1e-3	1e-2
	Lion	0.9	0.99	–	1e-3	1e-2
	Grams	0.9	0.999	–	1e-3	1e-2
Tuned						
ResNet-34	AdamW	0.9	0.99	–	1e-3	1e-2
	Adan	0.92	0.92	0.99	1e-3	1e-2
	Ano	0.95	0.995	–	1e-4	1e-2
	Lion	0.9	0.99	–	1e-4	1e-2
	Grams	0.9	0.999	–	1e-3	1e-2
Natural Language Processing (GLUE)						
Baseline						
BERT (base)	AdamW	0.9	0.999	–	2e-5	1e-2
	Adan	0.98	0.92	0.99	2e-5	1e-2
	Ano	0.92	0.99	–	2e-5	1e-2
	Lion	0.9	0.99	–	2e-5	1e-2
	Grams	0.9	0.999	–	2e-5	1e-2
	Anolog	–	0.999	–	2e-5	1e-2
Tuned						
BERT (base)	AdamW	0.9	0.99	–	7e-5	1e-2
	Adan	0.95	0.92	0.96	7e-5	1e-2
	Ano	0.92	0.999	–	2e-5	1e-2
	Lion	0.9	0.99	–	7e-6	1e-2
	Grams	0.9	0.999	–	7e-5	1e-2
	Anolog	–	0.999	–	2e-5	1e-2
Deep Reinforcement Learning (MuJoCo & Atari)						
Baseline						
SAC	Adam	0.9	0.999	–	3e-4	–
	Adan	0.98	0.92	0.99	3e-4	–

Table 10 (continued)

Model	Optimizer	β_1	β_2	β_3	lr	λ
	Ano	0.92	0.99	–	3e-4	–
	Lion	0.9	0.99	–	3e-4	–
	Grams	0.9	0.999	–	3e-4	–
	Anolog	–	0.999	–	3e-4	–
Tuned						
SAC	Adam	0.95	0.999	–	3e-4	–
	Adan	0.98	0.92	0.98	3e-3	–
	Ano	0.95	0.99	–	3e-4	–
	Lion	0.92	0.99	–	3e-4	–
	Grams	0.9	0.95	–	3e-3	–
	Anolog	–	0.999	–	3e-4	–

E.2 SAC SETTINGS

Hyperparameter	Value
Total training steps	1,000,000
Discount γ	0.99
Soft update rate τ	0.005
Replay buffer size	10^6
Batch size	256
Learning starts	5,000 steps
Actor LR / Critic LR	see Tab 10
Policy update frequency	2
Target network update freq.	1
Entropy coeff. α (init)	0.2
Entropy autotune	✓
Max grad. norm (actor)	0.5
Logging interval	2048 steps

Table 11: SAC hyperparameters used in our MuJoCo experiments (values taken from the code).

E.3 PPO SETTINGS

Hyperparameter	**Value**
Total timesteps	10,000,000
Number of envs (N_{env})	64
Steps per rollout (N_{steps})	64
Batch size ($N_{\text{env}} \times N_{\text{steps}}$)	4096
Minibatches	4
Minibatch size	1024
Update epochs	4
Discount γ	0.99
GAE λ	0.95
Learning rate	see Tab 10
LR annealing	linear (enabled)
Advantage normalization	✓
Policy clip coef.	0.10
Value clip	✓
Entropy coef.	0.01
Value loss coef.	0.5
Max grad-norm	0.5
Target KL	none

Table 12: PPO hyperparameters used in our Atari experiments (defaults from code).